An Unusual Electron Count and Electron-Deficient Multi-Center Bonding in One Class of Intermetallics: The $BaAl_4$, $CaAl_2Zn_2$, $CeMg_2Si_2$ and FCC Al Structures

Chong Zheng and Roald Hoffmann*

Department of Chemistry and Materials Science Center Cornell University, Ithaca, NY 14853

Z. Naturforsch. **41b**, 292–320 (1986); received October 23, 1985

Intermetallics, Electron-Deficient Multi-Center Bonding

The structural types discussed may be thought of as being composed of two-dimensional layers cleaved out of the FCC lattice. Each layer has a square sublattice capped by apical atoms above and below four-fold hollows. The electronic structure of such an Al layer is constructed – it has eight low-lying bands per four Al, and two of these bands are localized in apical Al's, pointing away from the layer. On stacking, bonds are formed between apical Al's, leading to the pushing up of one Al_a-Al_a σ^* band, and a gap after 7 bands are filled. This is $BaAl_4$, with Al_4^{2-}. An alternative picture is of delocalized five-center six-electron bonding in each hollow, closely related to the electron deficient bonding in B_5H_9. The bonding in $CeAl_2Ga_2$ and $CeMg_2Si_2$ can be derived similarly, by perturbing the original $BaAl_4$ case. A rationale for switching from $BaAl_4$ to the $CeMg_2Si_2$ structural type for electron counts exceeding ~16 for four atoms is given. Finally we relate these arguments to the high cohesive energy of Al metal.

More than 50 years have elapsed since the first synthesis of $BaAl_4$ [1], **1**. Since then chemists, in their industrious search for new structures, trying to understand the abundance given to us in the microscopic arrangements of atoms in the solid state, have found to their amazement that over 400 compounds crystallize in this prototype [2]. And this does not count the variants on this structural type or close relatives to it [3], structures such as $CaBe_2Ge_2$ [4], $TlCu_4S_3$ [5], $BaPtSn_3$ [6], $SrZnBi_2$, $SrZnSb_2$ and $SrCuSn_2$ [7]. Physicists joined the march recently, the vast collections of compounds, especially the transition metal intermetallics, providing them with an inexhaustible base for measurements, characterization, and ultimately understanding. The "heavy fermion" material $CeCu_2Si_2$ [8] and the high temperature silicide superconductors $Lu_2Fe_3Si_5$ (T_c = 6.0 K), $La_2Rh_3Si_5$ (T_c = 4.4 K) [9] are perhaps the most intriguing, but only two examples among many.

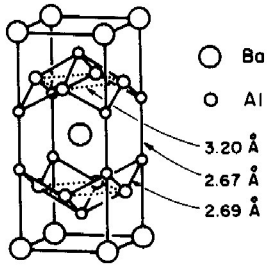

1

Despite the fact that so much experimental and theoretical effort has been devoted to the investigation of the $BaAl_4$ derivatives, the chemical bonding in the original phase still awaits elucidation. In this contribution we are going to analyze the bonding in the $BaAl_4$ and the closely related $REAl_2Ga_2$ [10], $CaAl_2Zn_2$ [11] and $CeMg_2Si_2$ [12] structures, with the assistance of extended Hückel type band calculations (details in Appendix).

The $BaAl_4$ Structure

The body-centered tetragonal $BaAl_4$ structure is shown in **1**. Motivated by our eventual analysis of the bonding in bulk Al metal, we would like to make a connection between the $BaAl_4$ structure and Al metal. **2** shows a "cleavage" of the Al FCC metal which allows us to see such a connection by inserting the Ba atoms [13]. A subsequent relative shift in the horizontal direction among layers makes additional interlayer Al–Al bonds, and the Al_4^{2-} part of the $BaAl_4$ 3-dimensional lattice is formed (**3**).

* Reprint requests to Dr. R. Hoffmann.

Verlag der Zeitschrift für Naturforschung D-7400 Tübingen
0340–5087/86/0300–0292/$ 01.00/0

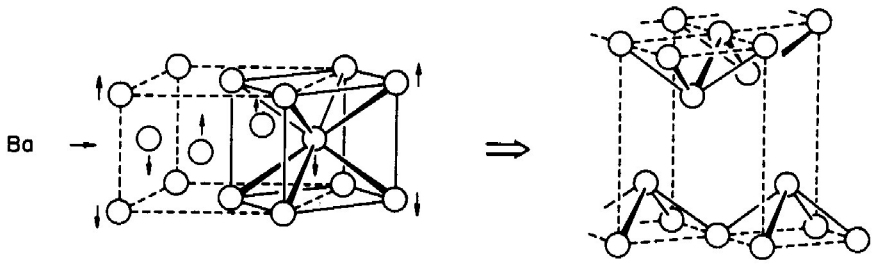

2

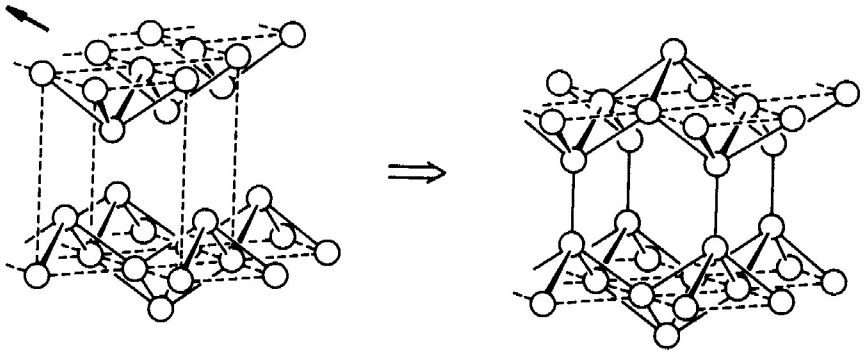

3

Let us describe the resulting structure in terms of sublattices. There are in the $BaAl_4$ structure obvious Ba layers, and two kinds of Al. One Al forms a square layer sublattice, with long 3.20 Å contacts within the square layer. We'll call these basal aluminums, Al_b. The square layers are capped on top and on bottom with the other kind of aluminum, which sit above and below the four-fold hollow sites of the square lattice. We will call these apical aluminums, Al_a. The Al_a–Al_b distance is short, 2.69Å (compare Al metal, where Al–Al is 2.86 Å). The two-dimensional layers are tied together by vertical Al_a–Al_a bonds, and these are again short, 2.67 Å.

The coordination around Al_b is approximately tetrahedral, not counting the four $Al_b \cdots Al_b$ contacts. Such an environment for a group 3 or 13 element is not unusual. But the coordination around the apical Al, Al_a, is different, for it is clearly five-coordinate, square-pyramidal. There are some consequences of this.

The Zintl Electron Count for $BaAl_4$

There are about a dozen or so compounds which adopt the $BaAl_4$ structure. Most of them are combinations of the alkali metal, alkaline earths or the rare earth elements with Group 13 elements [15], with 13 or 14 electrons per unit cell. An exception is $ThZn_4$ [16], which has 12 valence electrons if we count Th as Th^{4+}. These compounds are listed in **4**, reproduced from ref. [17].

From **4** we see that the atomic size ratio varies quite a lot, from 1.34 for $ThZn_4$ to 1.65 for $BaGa_4$. The electron count, on the other hand, is remarkably

A	X
Th	Zn
Ca Eu Sr Ba	Al
Na YbCa Eu Sr Ba	Ga
Ba K Rb	In

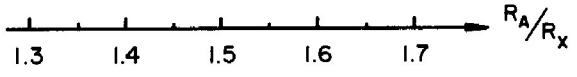

4

constant. Group 14, 15 phases, *e.g.* KGe_4, $RbGe_4$, KSn_4, KPb_4 [18], which have 17 or more electrons have not been found to crystallize in the $BaAl_4$ structure.

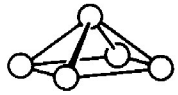

5

Thus, there *must* be some electronic driving force at work. The optimum electron count for the $BaAl_4$ structure should be around 14 per unit cell, judging from the known compounds. It is important that such an electron count is not obvious on the basis of the tremendously useful classical Zintl electron counting scheme, which assumes donation of electrons from the cations to the anions and bond formation among the anions to complete the octet [19]. Let us take an Al_5 square pyramid, **5** out of the $BaAl_4$ lattice for scrutiny. We see that there are four short bonds (2.69 Å) from the apical to the basal atoms, which comprise the 2-dimensional square lattice in the $BaAl_4$ structure. One would be led to think that eight electrons would be needed for these four bonds. Another short bond present between the apical atoms of two such pyramids requires two electrons, or one electron per square pyramid, adding up to nine electrons per square pyramid. The square pyramid corresponds to two Al atoms in the $BaAl_4$ lattice, since each basal atom in the pyramid is shared with four other pyramids. Thus 9 electrons per two Al's or 18 per $BaAl_4$ formula are required by Zintl's rule. Obviously this is not the case, for there are no such 18 electron compounds. The obvious five coordination of one Al calls for a multi-center delocalized description; the actual electron count of 14 electrons/4 atoms for electron deficient bonding. And the structure is inherently 3-dimensional, so a band structure is called for. We will see eventually how these three descriptions merge.

The Band Structure of $BaAl_4$

We will now build up the band structures step by step, first constructing the square lattice **6** and then the two-dimensional layer **7.** After that we proceed to the three-dimensional Al_4^{2-} lattice **8** by stacking the two-dimensional ones. Finally we may insert Ba^{2+} into the lattice.

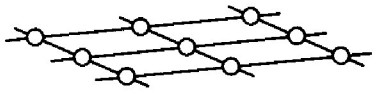

6

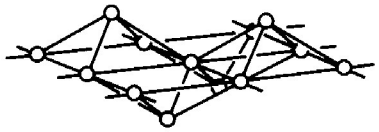

7

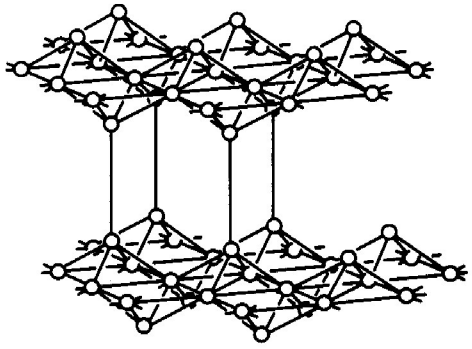

8

The band structure of a two-dimensional square lattice is most easily understood when the s band and p bands do not overlap, as shown in Fig. 1. At the Γ point in the Brillouin zone each orbital has the same phase as its four nearest neighboring translational correspondents. At the X point two nearest neighbors in x direction have the opposite phase, at the M point all the four nearest neighbors have the opposite phase. Thus the s band goes up in energy from Γ to X to M, as the number of the nearest bonding partners of the s orbital decreases from 4 to 2 to 0 (and the number of antibonding ones increases from $0 \rightarrow 2 \rightarrow 4$). The p_z band, topologically the same as the s band, changes its energy in a similar fashion; only the band width is much smaller due to the less effective π type overlap between the nearest neighbor p_z orbitals. The p_x and p_y bands are degenerate at Γ, both having 2 antibonding σ interactions and 2 bonding π interactions with their nearest neighbors. Upon going away from Γ to X where 2

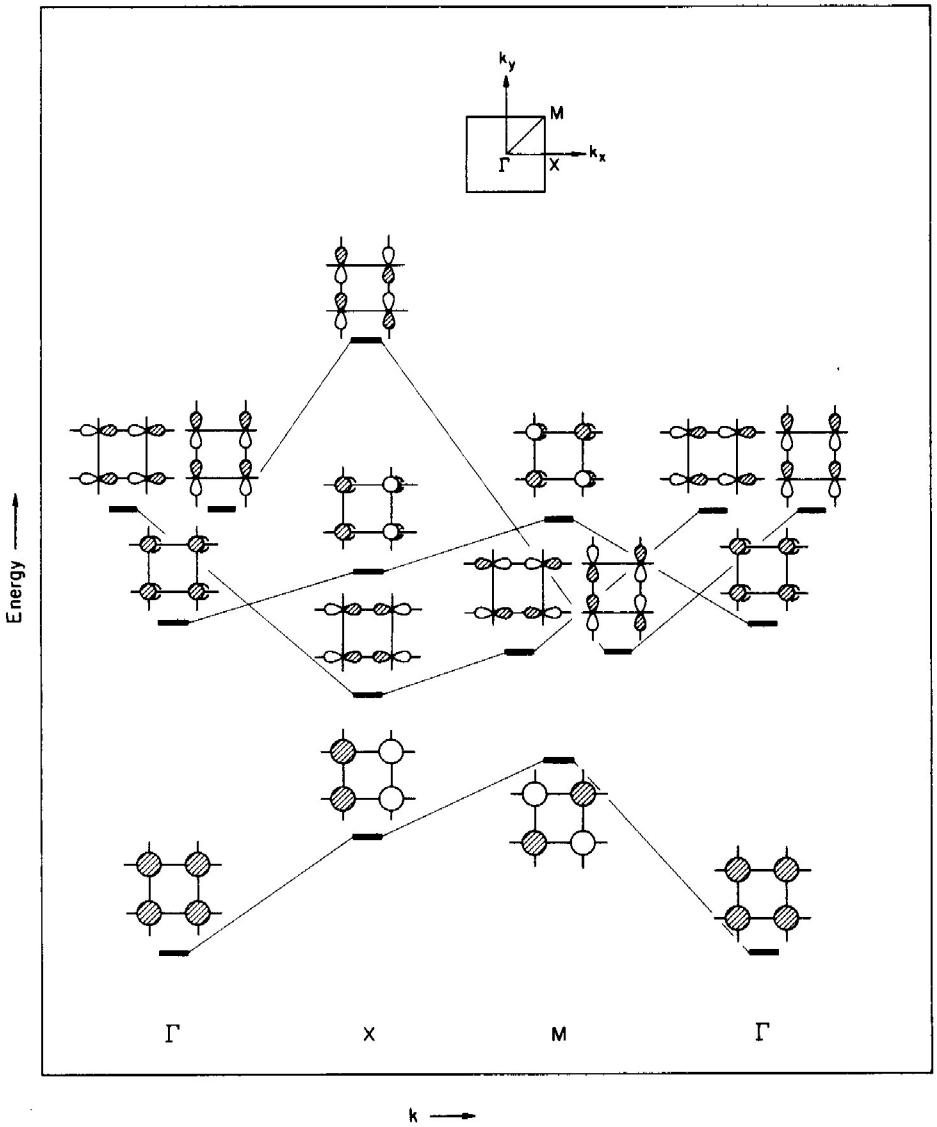

Fig. 1. Schematic band structure of a planar square lattice. The s and p levels have a large enough separation so that the s and p bands do not overlap.

nearest neighbors along the x direction have the opposite phase, the degeneracy is broken. The p_x band goes down in energy when the antibonding neighbors along the x direction become bonding ones; the p_y band rises up due to the π antibonding character along the x direction. They meet again at M where both bands have 2 σ bonding and 2 π antibonding nearest neighbors.

Fig. 2 is the calculated band structure of a two-dimensional Al square lattice with an unrealistically large lattice constant $a = 4.5$ Å. The shape of the bands is that expected from the preceding discussion. If the lattice constant is smaller, and therefore the inter-cell overlap greater, the band structure should appear somewhat different; the s band being likely to cross the p bands. Structure **9** indicates schematically what is likely to happen, with the s band at M (four out-of-phase nearest neighbors) higher than the p bands. Avoided crossings occur between the s band

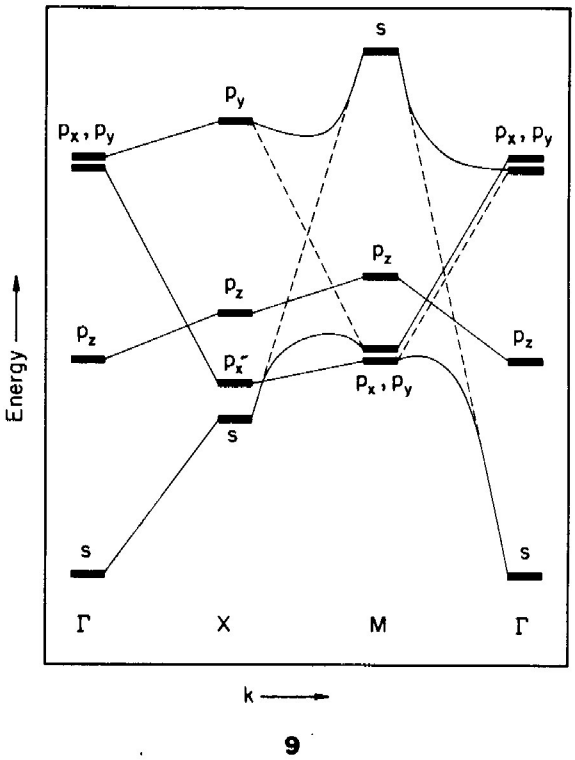

9

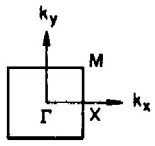

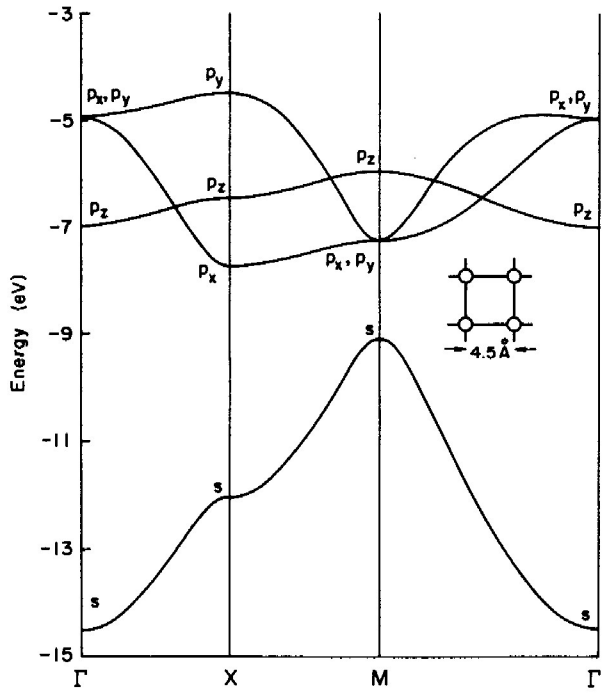

Fig. 2. Band structure of a square lattice of Al atoms. The lattice constant is deliberately chosen to be big enough ($a = 4.5$ Å) so that the s and p bands do not overlap.

and p_y (X→M) or $p_x + p_y$ band (M→Γ), since they all have the same symmetry in the group of k. The p_z band, being *anti*-symmetric with respect to the plane of the square lattice, does not mix with any other bands. Fig. 3 is the calculated realization of **9**, a band structure of the square lattice in $BaAl_4$ ($a = 3.2$ Å).

Since the layers in $BaAl_4$ have only a glide plane parallel to the layer instead of a real mirror plane, we need to classify the levels according to their symmetry with respect to the glide plane. Otherwise, we have to choose 4 Al atoms (instead of 2) as a unit cell and the band structure analysis becomes more complicated. The glide plane is a reflection in the plane of the paper and a translation along x direction, taking an atom at position 1 to 2 in **10.**

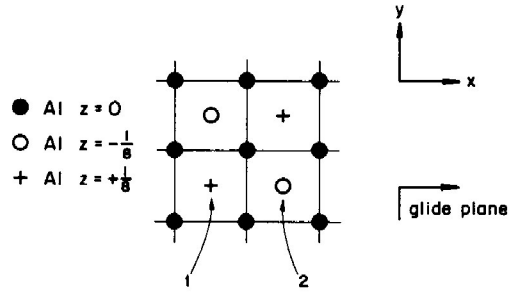

10

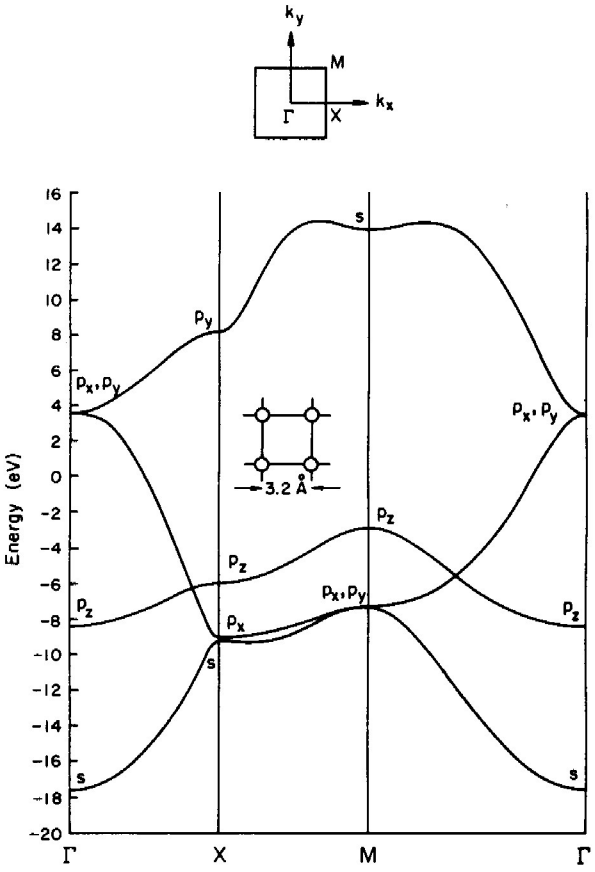

Fig. 3. Band structure of the Al square lattice taken from $BaAl_4$. The s band crosses the p bands due to the high dispersion produced by a small lattice constant ($a = 3.20$ Å).

In the Bloch sum $\hat{P}\phi$ where $\hat{P}$ is the projector $\hat{P} = \sum_{\mathbf{R}} e^{i\mathbf{k}\cdot\mathbf{R}}\hat{T}_{\mathbf{R}}$ and ϕ an arbitrary function the symmetry operation $\hat{T}_{\mathbf{R}}$ can be something other than translation, as long as $\{\hat{T}_{\mathbf{R}}\}$ is Abelian and represented by $\{e^{i\mathbf{k}\cdot\mathbf{R}}\}$. In our case $\hat{T}_{\mathbf{R}}$ is the glide plane (or the two-fold screw axis) and $\mathbf{k}$ is no longer plane wave but contains angular parts. There have been some previous applications of this idea where the asymmetric unit is chosen as the "unit cell", so as to simplify the calculations for biological [20a–d] and solid state systems [20e].

One choice of the unit cell is **11**, where a_2 is the conventional lattice translation vector but a_1 the glide plane translation. The unit cell (shaded area in **11**) contains two Al atoms, one from the planar square lattice ($z = 0$) and the other from the apex above the hollow of the square lattice ($z > 0$). We

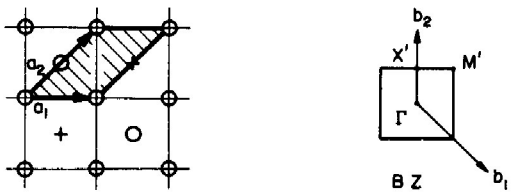

11

need to replot the bands in Fig. 3 from $\Gamma \rightarrow X' \rightarrow M' \rightarrow \Gamma$ in the Brillouin zone (BZ) defined in **11**, in order to prepare the square lattice to interact with the apical atoms.

Fig. 4 shows such a plot. All the bands which are symmetric with respect to the plane containing the square lattice (s, p_x, p_y) remain unchanged. The p_z band, however, changes its appearance. This is due

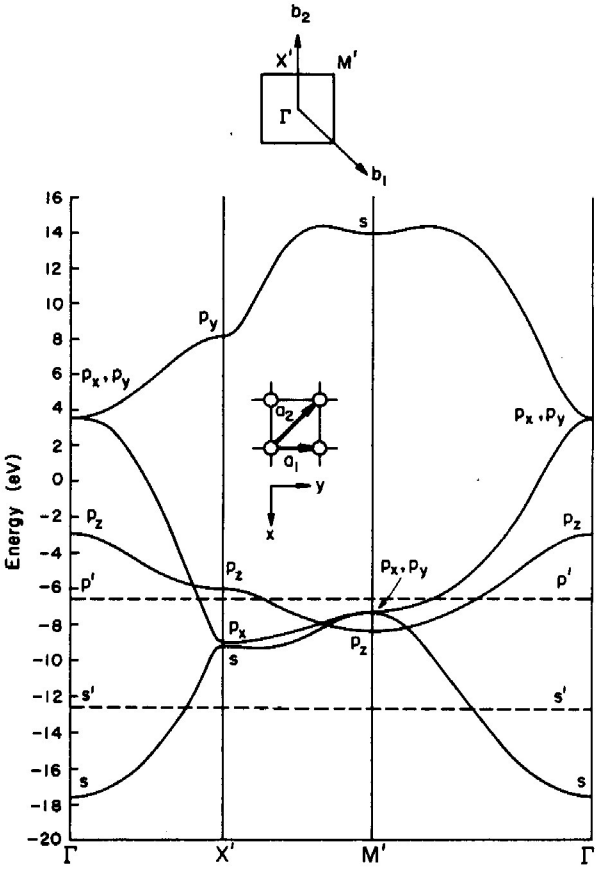

Fig. 4. Glide plane band structure of the Al square lattice taken from $BaAl_4$ (*cf.* Fig. 3). The dashed lines indicate the atomic s and p levels.

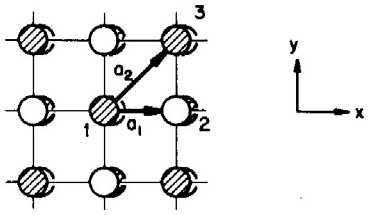

12

to the fact that we plot the glide plane band structures along a_1 instead of a simple translation. An example is **12**, the p_z band at Γ. The phase relation is now determined by the glide plane along a_1 and simple translation along a_2. The p_z orbitals at sites 1 and 2 are in-phase with respect to the glide plane along a_1, since the glide plane reverses the z direction. Sites 1 and 3 are in-phase by the translation a_2. Thus **12**, the Γ point of the BZ in **11**, corresponds to M in the conventional BZ, illustrated in Fig. 1. Similarly, X', **13**, M', **14**, correspond to X and Γ points in Fig. 1.

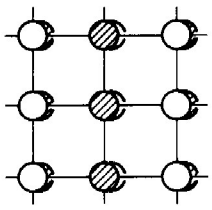

13

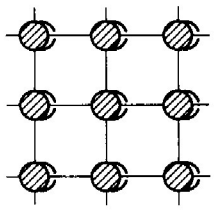

14

The other orbitals s, p_x, p_y are in the plane of the square lattice and unaffected by reflection in that plane. It is important to note that in plotting the glide plane band structures no information is lost – we just plot the p_z band in a different way.

We are ready at this stage to interact the square lattice with the apical atom. The dashed lines around −12.3 and −6.5 eV in Fig. 4 indicate the s and p levels of an (apical) Al atom. The states of the square lattice above these levels will act as acceptors, being pushed up when the composite layer **7** is formed. We illustrate what will happen upon interaction of square (basal) and apical sublattices in Fig. 5.

On the left side in Fig. 5 we plot the approximate band structures (heavy lines) for the square lattice from Γ to M' (*cf.* Fig. 2): the s and p_y bands rise up, the p_x band drops sharply, the p_z band, when plotted against the glide plane we mentioned before, sinks very slowly. The p_x and p_z bands, being of different symmetry with respect to the plane **m** shown in **15** (in the group of k from $\Gamma \rightarrow$ X'), cross each other.

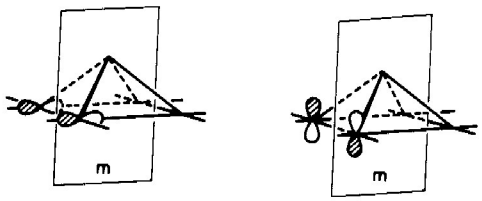

15

The s and p levels of the apical atom, denoted by s', p', are between the s and p_z bands before the apical-basal interaction is turned on. When the interaction is turned on, the square lattice bands will mix with the basal orbitals of the correct symmetry as depicted in Fig. 5. As a consequence, these levels will shift. At Γ the s band has the right symmetry to interact with s' and is pushed down in energy, as indicated by the arrow. s' is lifted up, but p_z', being of the same symmetry, will mix with s', preventing s' from rising further. So we'd expect s' to remain approximately the same in energy, and p_z' goes up as indicated by the arrow. p_x', p_y' interact with p_x, p_y bands at higher energy. p_x', p_y' are pulled down and p_x, p_y up. The p_z band at Γ, being of δ type symmetry, does not interact with any of the apical orbitals.

At the X point the s band interacts with the p_x' and is pulled down. p_x' is lifted up consequently. s' can interact with p_x', thus s' goes down and p_x up in energy. A similar interaction governs p_y', p_z and p_z'.

On the right side in Fig. 5 are the levels after the shifts indicated by the arrows are accomplished. Now we need to connect the bands from the lowest level up to obtain the approximate band structure. It should be pointed out that when the apical atom is in place, the group of k from Γ to X' contains only the identity operation. All the bands have the same symmetry and they do not cross each other. This is because the original mirror plane **m** in **15** no longer

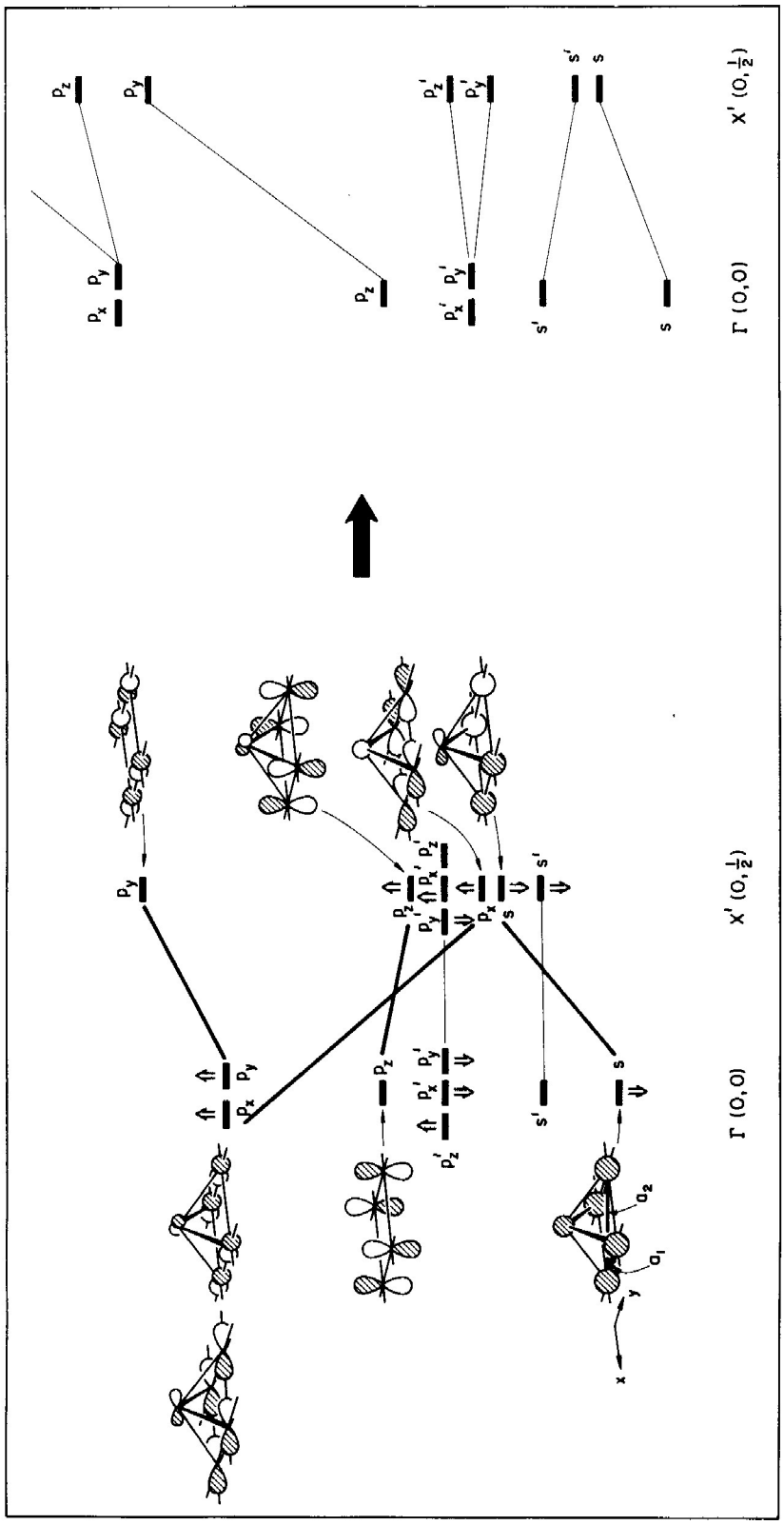

Fig. 5. A schematic interaction diagram for the two-dimensional layer in $BaAl_4$ as formed from a square lattice and apical atoms. On the left is the band structure *before* the $Al_a - Al_b$ interaction is turned on. The bands of the square lattice are shown in heavy lines, and the apical atomic levels in light lines. Only square lattice orbitals are drawn and combined with the apical orbitals to indicate the symmetry match. The arrows indicate the directions in which those levels should shift *after* the $Al_a - Al_b$ interaction is turned on. On the right side are the bands obtained after the level shift.

exists. The phase relation between sites 1 and 2 in **16** is determined by the k value and independent of the mirror plane.

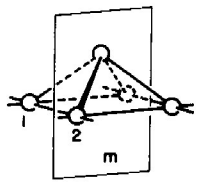

16

Before we connect the bands, we should notice that at both Γ and X′ points 3 bands are pulled down and 1 remains approximately the same. The others are either pushed up high or are originally high in energy. Thus, the connection of bands is most easily accomplished. The four lowest bands are connected, then there should be a gap. This is shown at the right side of Fig. 5.

From X′ to M′ and from M′ to Γ the construction is similar, and we will not present it here. Suffice it to say that simple bonding symmetry and overlap arguments allow us to derive with ease the qualitative features of the band structure throughout the Brillouin zone. In all directions there are four low-lying bands, and a gap to a 5th band. The four lower bands are all apical-basal bonding, and are bonding or nonbonding within the square lattice. Antibonding within the square lattice would come about through orbitals of δ symmetry, and these are not stabilized by apical-basal interaction.

When the four bands are filled, we reach an electron count of 8 electrons per 2 Al, or Al_2^{2-}. Note this is 16 electrons per 4 Al, *i.e.* we have not yet obtained an explanation of the magic 14 electron count. But then we have not yet built the three-dimensional solid, only a two-dimensional slice of it.

The calculated band structure, the corresponding density of states (DOS) and crystal orbital overlap population (COOP) curves are drawn in Fig. 6. The band structure shows the anticipated characteristics. The DOS curve also shows the contribution of basal aluminums of the total DOS. What is not on Al_b is on Al_a.

As implied by the band structure of the square lattice alone, Fig. 4, many square lattice states lie higher than the apical atom levels. When the interaction between the square lattice and the apical atoms is turned on, more square lattice states will be pushed up than apical ones. Thus, below the gap there are less square lattice states. The contribution up to the gap around −4 eV from the square lattice to DOS in Fig. 6 is less than 40%, what is left over (>60%) in the total DOS is from the apical atoms. Hence the apical atoms are more negatively charged than the square lattice ones when the lowest 4 bands of the layer are filled. The charge imbalance also can be understood from another point of view, based on dispersion of the filled and unfilled bands [21].

The COOP curve shown in Fig. 6 is an overlap population weighted density of states, and a nice index of the bonding character of a given bond [22]. Below the gap at −4 eV, nearly all the states are Al_a–Al_b bonding, but above the gap strong antibonding features develop. An electron count above Al_4^{4-} would be most unfavorable.

Before we go on to the three-dimensional lattice, we need to "fold back" the band structures [23] so that there will be 4 Al atoms per cell and 16 bands altogether. The band structures are then not plotted against the glide plane but the conventional k vectors generated by the translations. In this way we prepare the bands for interaction in the third dimension [24].

17 and **18** show the folding-back process. In a one-dimensional system a line is folded back, in two-

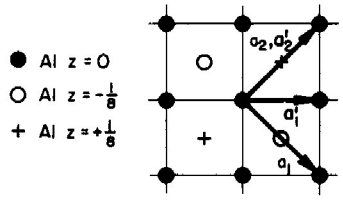

17

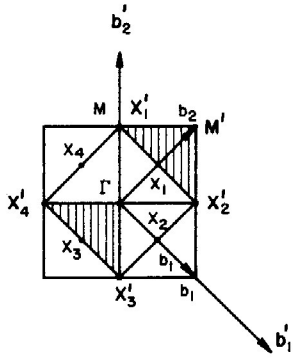

18

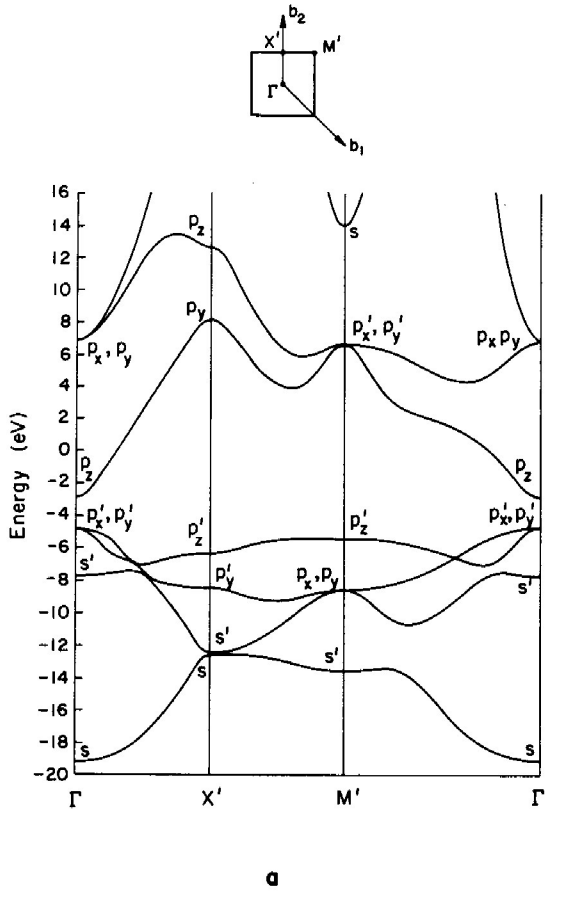

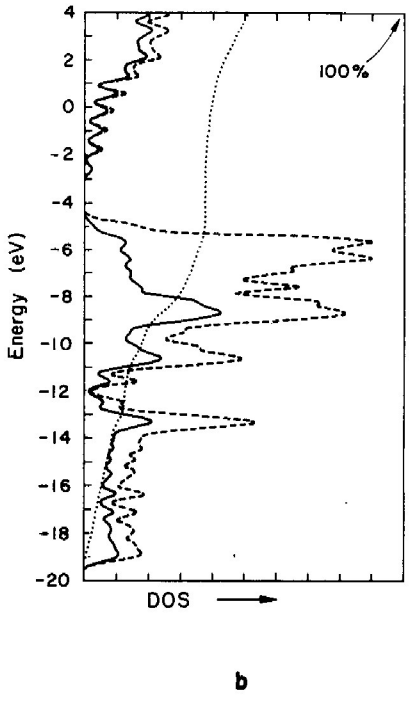

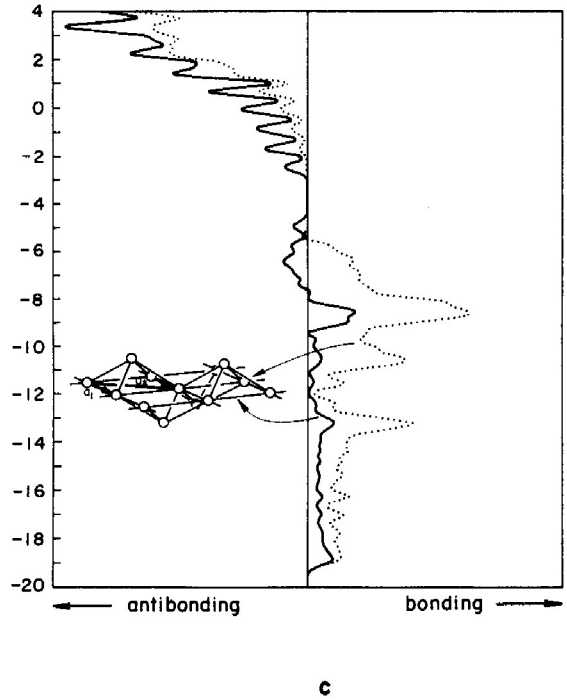

Fig. 6. (a) Band structure of the two-dimensional layer taken from $BaAl_4$. The bands are plotted against the glide plane so there are two Al atoms per unit cell. The main contributions to the bands are indicated at each special k point: s, p for the basal Al_b and s', p' for the apical Al_a. (b) Total density of states (dashed line) and the basal Al_b contribution (solid line) for the two-dimensional layer in $BaAl_4$. The dotted line is the integrated Al_b state density. (c) Crystal Orbital Overlap Population curves for the two-dimensional layer in $BaAl_4$. Solid line: Al_b–Al_b bond; dotted line: Al_a–Al_b bond.

dimensions an area and in three-dimensions a volume. **17** is the direct lattice. We choose a_1' (glide plane translational vector) and a_2' to define the unit cell which contains 2 atoms (**11**). The corresponding reciprocal vectors are b_1' and b_2' in **18** which are perpendicular to a_2, and a_1', respectively. The Brillouin zone is the big square in **18.** If we choose the conventional unit cell defined by a_1, a_2 which contains 4 atoms, the corresponding reciprocal vectors will be b_1, b_2, perpendicular to a_2, a_1, respectively. The Brillouin zone $X_1'X_2'X_3'X_4'$ in **18** is half the size of the Brillouin zone defined by b_1', b_2', since in the direct lattice the unit cell is doubled.

If we choose the conventional unit cell (a_1, a_2), the triangular area $X_1'M'X_2'$ will be outside the Brillouin zone (b_1, b_2) but can be translated back into the zone ($X_4'\Gamma X_3'$) by b_2. Thus the line $X_1'M'$ corresponds to $X_4'\Gamma$ which in turn corresponds to ΓM by the 4-fold symmetry in the direct lattice. Similarly $M'X_1$ corresponds to ΓX_3 and in turn to ΓX_1 by time reversal. In other words when we fold $\Gamma X'$ onto $X'M'$ and fold $M'\Gamma$ back such that Γ coincides with M' in Fig. 6, what we get is the band structure from M to Γ to X for the conventional cell (a_1, a_2). This process is shown in Fig. 7. It results in 8 low-lying bands for 4 Al atoms in the unit cell (a_1, a_2).

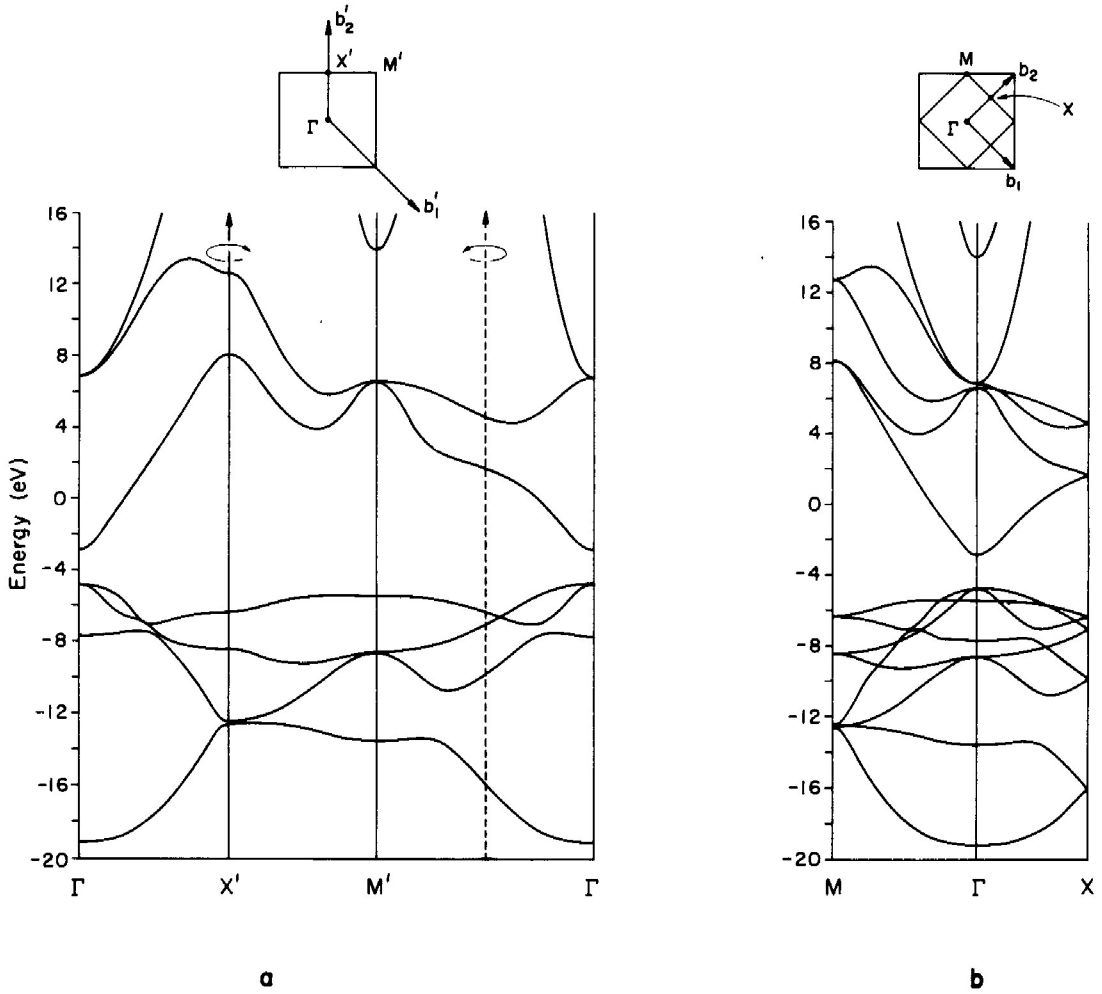

Fig. 7. Band structures of the two-dimensional layer in $BaAl_4$ before (**a**) and after (**b**) the "folding back" process is performed. The arrows in **a** indicate the "rotation axes" for this folding back process.

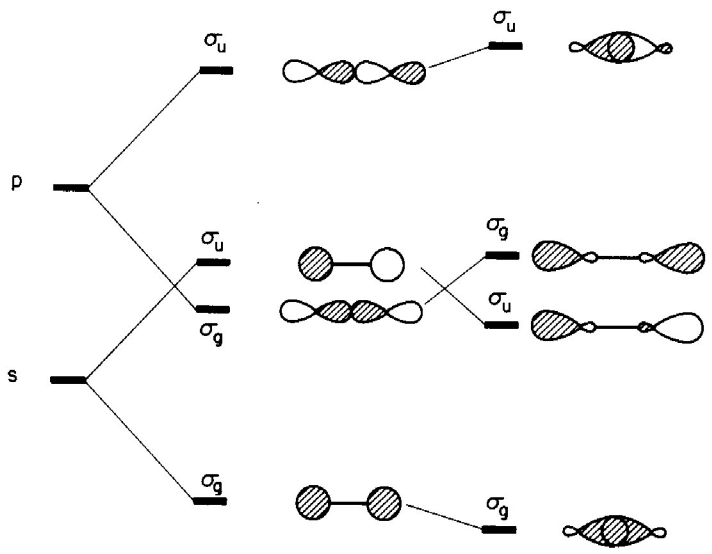

19

In the folded band structure Fig. 7b there are 4 bands which are mainly of apical s′ and p_z′ character, as we outlined earlier in our derivation. Thus when the two-dimensional layers **7** are stacked to form the three-dimensional lattice **8** these 4 bands should result in 2 bonding and 2 antibonding combinations. The actual situation is complicated a little, by mixing between s′ and p_z′ upon stacking. What happens is analogous to s, p hybridization in a diatomic, sketched in **19.** The mutual mixing of the symmetry-adapted σ_g and σ_u combinations formed from 2 s and 2 p_z respectively, transforms the σ_g (2 s) and σ_u (2 p) orbitals into strongly bonding MO's, but makes σ_u (2 s) and σ_g (2 p) more or less non-bonding.

Something very similar happens for the s′ and p_z′ bands in the $BaAl_4$ structure. As **20** shows, one obtains $\sigma_{s'}$ (bonding) $\sigma_{s'}$* (nonbonding), $\sigma_{p_z'}$ (nonbonding) and $\sigma_{p_z'}$* (antibonding). The p_x′, p_y′ bands should not be disturbed too much, due to their poor inter-layer overlap.

Fig. 8 shows the band structure, DOS and COOP of the three-dimensional lattice **8.** Below the gap around −4 eV there are two s′ and one p_z′ bands, corresponding to $\sigma_{s'}$* and $\sigma_{p_z'}$ in **20.** The other band, equivalent to $\sigma_{p_z'}$* is pushed up high above the gap because of its strong antibonding. Below the gap there are 7 bands now which can accommodate 14 electrons from $BaAl_4$.

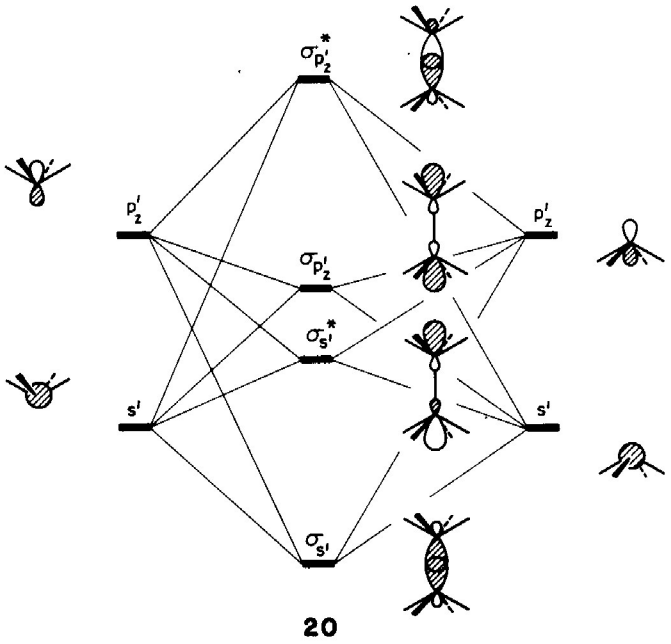

20

From our construction these seven bands should be mostly Al–Al bonding. The COOP curves in Fig. 8 confirm this. There is Al–Al bonding everywhere below the gap, except for an interesting small Al_b–Al_b antibonding bump just below the Fermi level. An electron count greater than 14 would

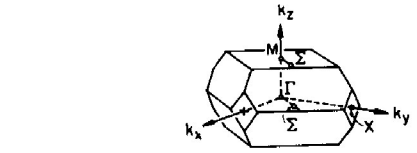

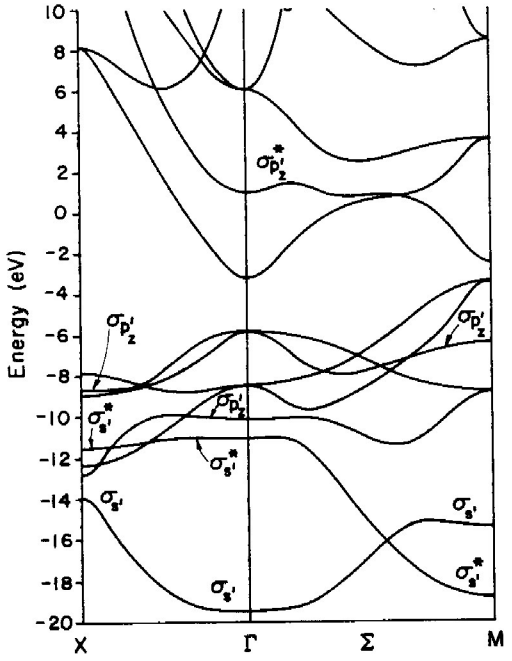

a

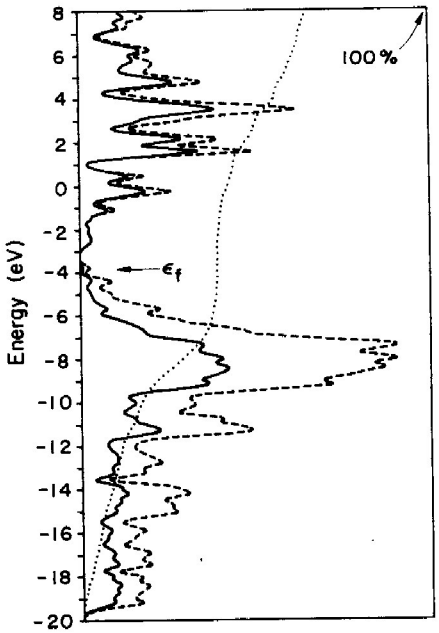

b

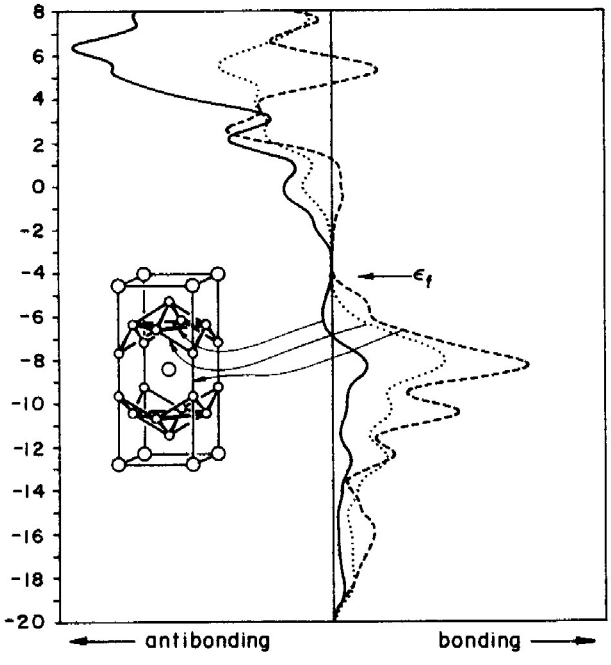

c

Fig. 8. (a) Band structures of the three-dimensional Al latice in $BaAl_4$. The apical bands (s', p') are indicated at each special k point.
(b) Density of states of the same lattice (dashed line) and the basal Al_b contribution (solid line). The dotted line is the integration of the Al_b states.
(c) Crystal Orbital Overlap Population curves for the same lattice. Each curve corresponds to a specific bond as indicated in the picture.

quickly ruin all Al–Al bonding. We now understand clearly the 14 electron count characteristic of $BaAl_4$ structures.

We noted earlier the negative charging of the apical sites in one layer. As the relative contributions to the DOS in Fig. 8 show, this persists in the three-dimensional solid. The calculated charges for a 14 electron Al_4^{2-} structure are given in **21.** It follows that when two of the four Al's in $BaAl_4$ are substituted by an isoelectronic but more electronegative element, that this element should occupy the apical position [25]. Indeed, this is what is observed for $REAl_2Ga_2$ [10] (as it should be on the basis of a lattice site dispersivity argument as well [21]). Ga ($\chi = 1.81$) is more electronegative than Al ($\chi = 1.61$). The same is true for Zn ($\chi = 1.65$) [26] in $CaAl_2Zn_2$ so we expect Zn to be at the apical position, as it is.

21

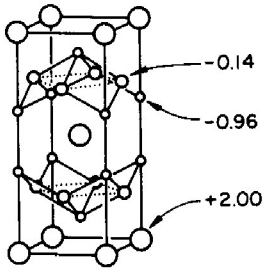

We search for a still simpler picture of the bonding in the solid, for a chemical explanation of the 14 electron count. Since the apical site is more appropriate for a more electronegative element let's think of $BaAl_4 \equiv Ba^{2+}[(Al_a)_2(Al_b)_2]^{2-}$ as $Ba^{2+}(Al_a^{4-})_2(Al_b^{3+})_2$, *i.e.* transfering all the electrons to Al_a. Remember, this is just a formalism, Al_a^{4-} is isoelectronic with Cl. So the short interlayer bond, a full single bond, is easily understood. What about the Al_a–Al_b bonding? Let us form tetrahedral hybrids at each Al_b, pointing to the neighboring Al_a. But at each Al_a let's form instead sp hybrids, one of which is then involved in the apical Al_a–Al_a bond. The basis functions are shown in **22.**

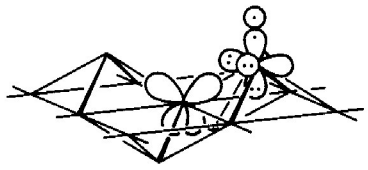

22

In each hollow there will be four hybrids, one from each Al_b around the hollow, pointing towards Al_a. The cyclobutadienoid symmetry-adapted linear combinations are easy to draw, and so is the hollow interaction diagram, **23.** Three delocalized bonding

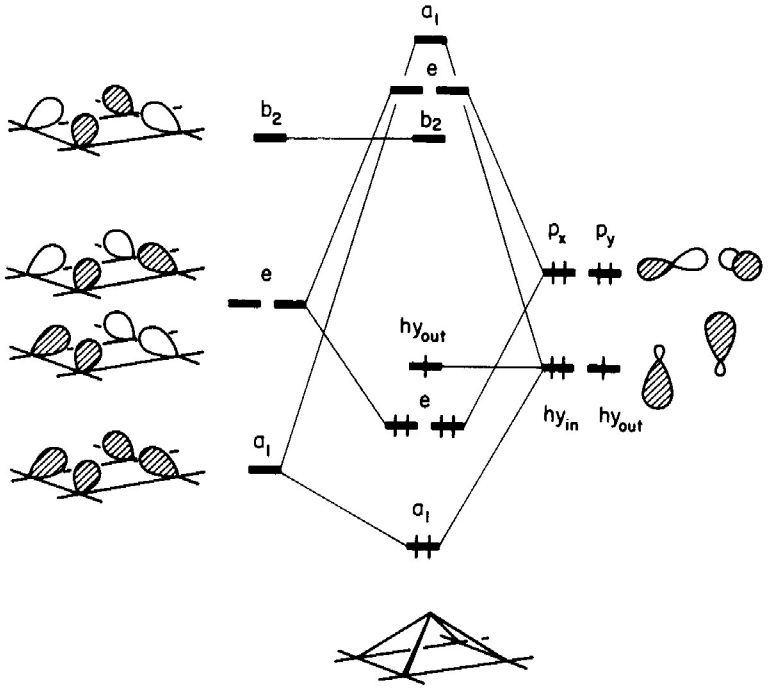

23

MO's are formed, of $a_1 + e$ symmetry. These are responsible for $Al_b - Al_a$ bonding. The seventh electron of $Al_2^- \equiv (Al_a^{4-})(Al_b^{3+})$ enters the sp hybrid hy_{out}, pointing away from the hollow. When the three-dimensional framework is assembled, this orbital and its electron are used to form normal two-center, two-electron bonds.

To summarize: the Al_4^{2-} framework of $BaAl_4$ is held together by 14 electrons per $(Al_a)_2(Al_b)_2$. Two of these electrons are involved primarily in $Al_a - Al_a$ bonding, the other twelve, six in each of two hollows, hold together Al_a and Al_b through electron-deficient multi-center bonding. Four $Al_a - Al_b$ bonds (not two-center, two-electron bonds) are made with only six electrons.

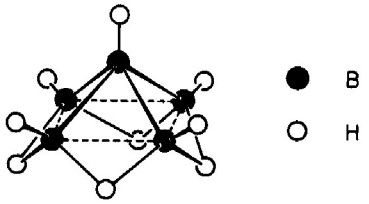

24

The type of bonding that is discussed here is nothing new. It is precisely the kind of bonding suggested in the boranes by Lipscomb [27, 28]. More directly, we have precise analogues for $BaAl_4$ in B_5H_9, **24**, and $B_{10}H_{16}$, **25**. In B_5H_9 each boron uses

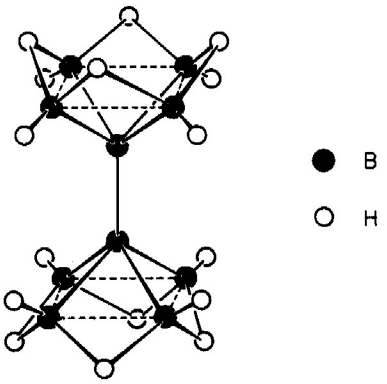

25

one electron for terminal H bonding. That leaves $5 \times 2 = 10$ electrons per five borons. Then the bridging hydrogens are held by four three-center, two-electron bonds, to which each basal boron contributes one electron, each hydrogen one. That leaves $10 - 4 = 6$ electrons for framework bonding. $B_{10}H_{16}$, **25** [29], is a still more direct analogue of the $BaAl_4$ structure.

Let us in summary trace what happens as we progress from a local viewpoint to the fully delocalized structure. Starting with sp^3 hybrids at Al_b and sp at Al_a we get the local (but delocalized, locally!) hollow MO's, **26**. At the right side we have doubled the Al_2

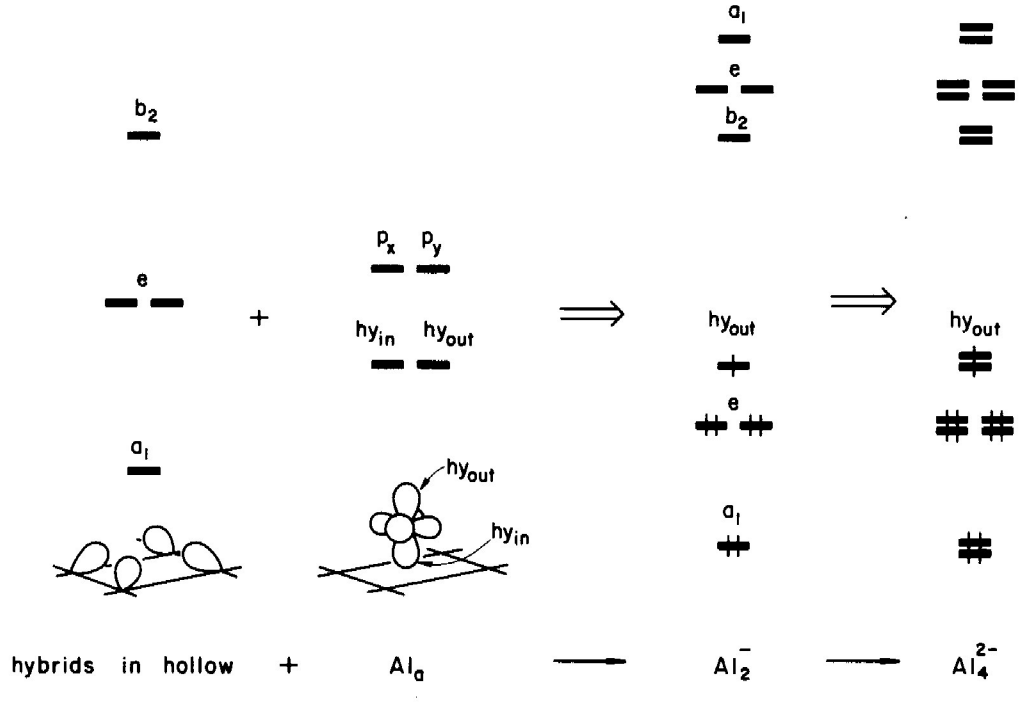

26

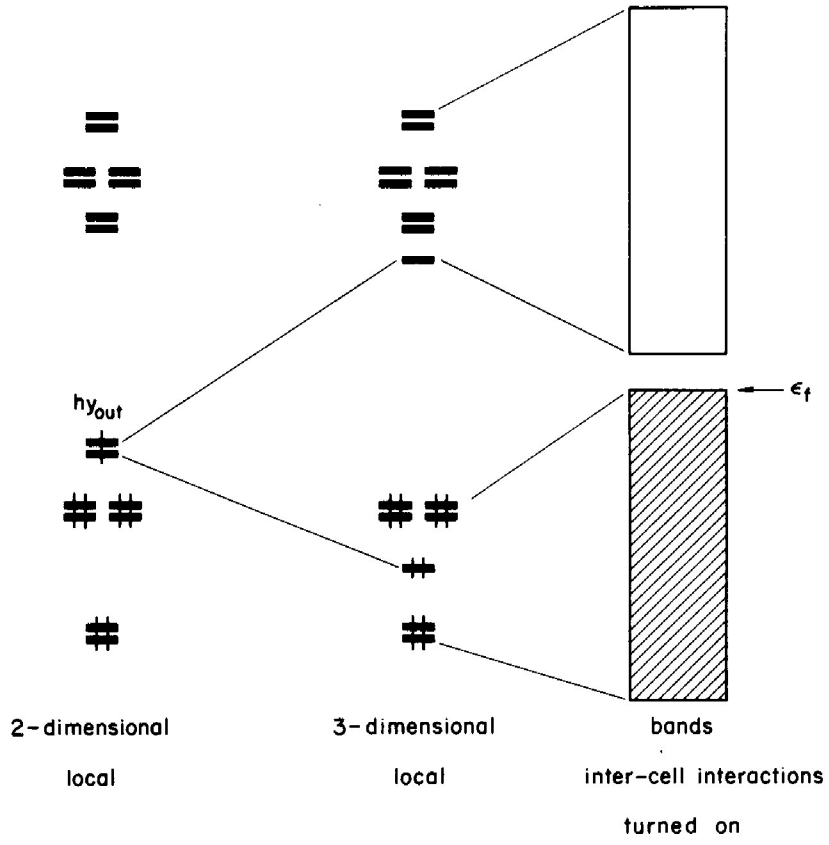

27

MO's to anticipate full unit cell. No hollow-hollow interaction is yet turned on.

Now we stack the layers. This turns on the localized two center bonding between Al_a's, but does little else, **27.** One orbital, Al_a-Al_a bonding, goes down, one Al_a-Al_a antibonding orbital goes up. A gap occurs after 7 levels, 14 electrons, Al_4^{2-}. Now we turn on the inter-unit cell interactions. (They could have been turned on earlier – remember this is just a schematic reconstruction of a complex process in which many things, within a unit cell and between unit cells, happen, all at once.) Each of the 14 levels develops into a band. But the inter-unit cell interactions, the delocalization, is not strong enough to destroy the locally imposed gap after the seventh level. A band gap remains after 14 electrons per unit cell.

To complete our discussion of $BaAl_4$ we should insert Ba^{2+} into the three-dimensional lattice. This will add to the total energy a Madelung contribution, but the occupied bands should not be perturbed too much since the Ba^{2+} levels are very high in energy. The dominance of different contributions to the total energy in different geometrical realizations of the lattice may sometimes lead to a double minimum and requires more sophisticated study.

The $CeMg_2Si_2$ Structure

The $CeMg_2Si_2$ structure [12], **28,** differs from the $BaAl_4$ structure in that half of apical atoms are

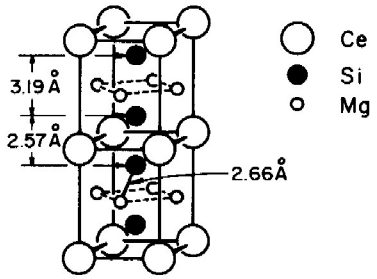

28

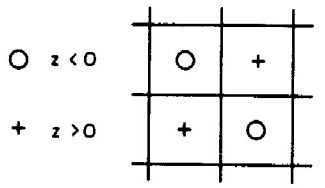

$BaAl_4$

29

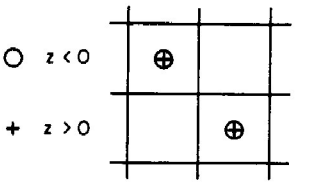

$CeMg_2Si_2$

30

shifted so that above and below one hollow of the square lattice there are two such apical atoms but in an adjacent hollow there is none, *cf.* **29, 30.** The apical positions are taken by the more electronegative Si atoms, as expected from lattice site dispersivity [21]. The Si–Si distance between the two-dimensional Mg_2Si_2 layers is 2.57 Å, but is longer within one layer, 3.19 Å. In other words, there is no Si–Si bond within a layer. We will construct the approximate band structure through a procedure similar to that used for the two-dimensional layers in $BaAl_4$, then stack the layers together to the three-dimensional lattice. We will use Al atoms first for a structural comparison, and then add the perturbation to derive the $CeMg_2Si_2$ bands. The simplest starting point is again the hybrids. For the hollow *with* apical atoms we use **23** (or **26**) as the bonding scheme, whereas for the hollow *without* the apical atom the orbital levels are trivial: they are just the original hollow hybrid levels (left side of **23** or **26**) before interaction with Al_a. In addition, we have an extra apical atom, interacting poorly with the two hollows. The schematic level diagram is shown in **31.** The levels for the hollow without the apical atom should

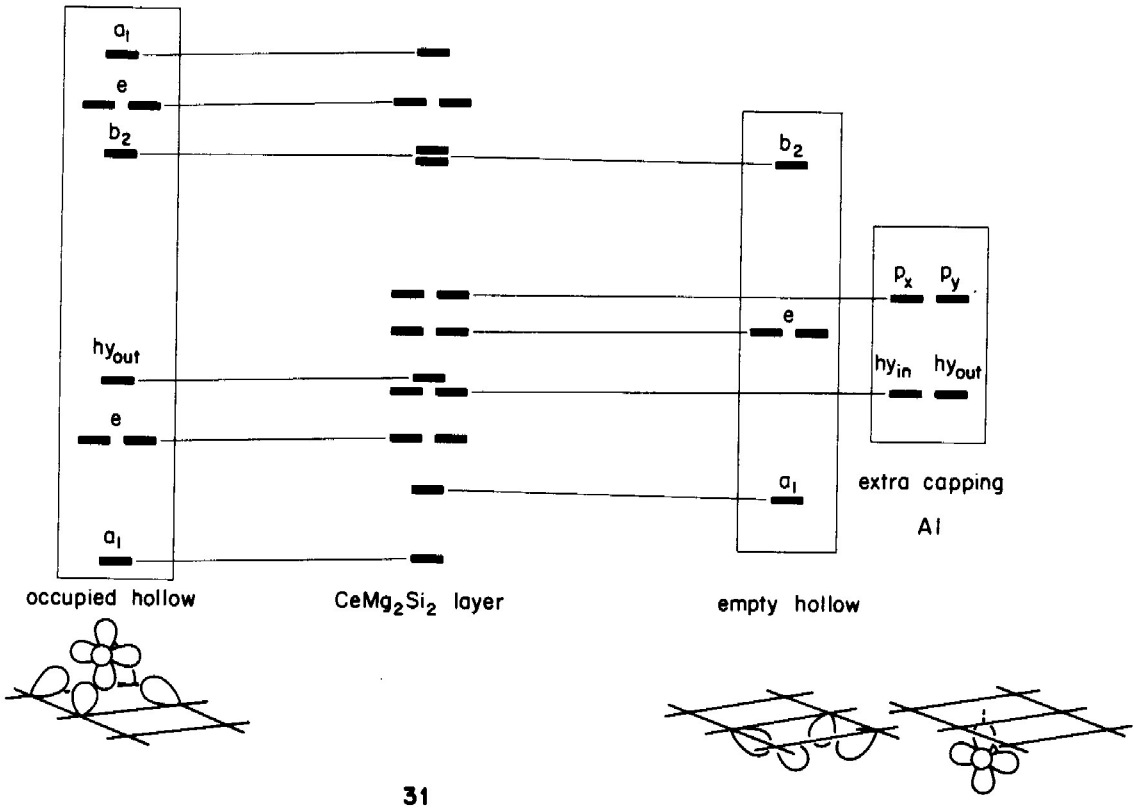

31

be in the gap of those for the hollow with the apical, for that gap is created by the interaction between the hybrids and the apical atoms, now absent in the empty hollow.

In the three-dimensional solid one level should be pushed up by the interlayer interaction and all the levels develop into bands, **32.** There should be no band gap in this case.

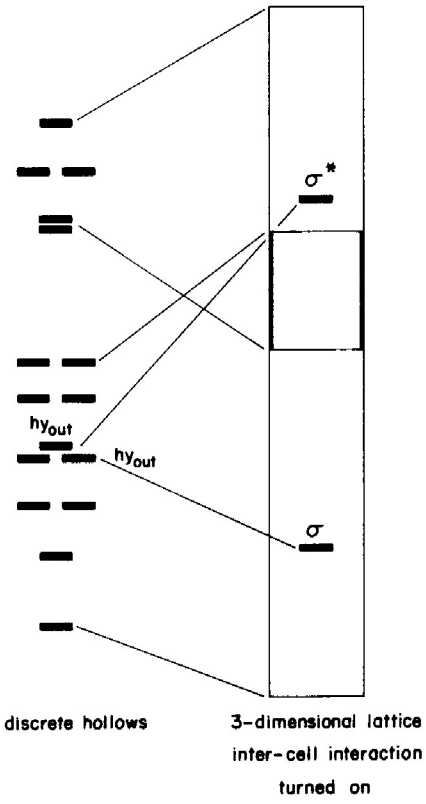

32

Let us see how these qualitative considerations check out in a full calculation. Fig. 9 shows the band structure and some projections of the DOS for a two-dimensional layer of Al atoms in the $CeMg_2Si_2$ slab **33.** The hollow size and the apical to basal Al–Al distance are kept the same as those in the $BaAl_4$ lattice. There is no band gap indeed. The two DOS curves show the full DOS and the contributions to it by the hybrids pointing toward the apical atoms (filled hollows) and away (empty hollows). For the filled hollow hybrids it is clear that there is a separation of these orbitals into two regions (see left side of **31**), with a gap between −6 and +6 eV. For the empty hollow hybrids there is a general smearing, delocalization throughout, but most of the states are in that gap.

We will not describe the detailed features of the band structure in Fig. 9. Instead we will sketch a part of it in order to illustrate the absence of an energy gap. The part we will explore consists of the bands from M to Γ which are antisymmetric with respect to the plane of the two-dimensional square lattice in **33.** Now there is a mirror plane of symmetry, containing the square lattice.

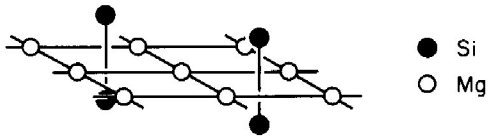

33

These bands are labeled "A" and drawn in a heavy line in Fig. 9. We will derive the approximate band structures again by interacting the square lattice bands with those of the apical atoms, as we did from Fig. 4 to Fig. 5.

In the Mg_2Si_2 type layer there is no such symmetry as the glide plane in the $BaAl_4$ layer that we can use to reduce the unit cell size. We have to use the bands corresponding to two Al atoms in the square lattice to interact with the apical atoms.

Fig. 10 is such a band structure, as derived by folding back the bands in Fig. 2 for the same square lattice but half the unit cell size (one Al atom per unit cell). The Brillouin zones for the two different choices of unit cells are the same as those shown in **17** and **18:** the big unit cell corresponds to the small Brillouin zone (BZ) and *vice versa.* In the folding back process the M point of the big BZ (*i.e.* small unit cell, Fig. 2) is folded back to the Γ point of the small BZ (large unit cell, Fig. 10). Similarly, the X_1 ($k_x = 0.5$, $k_y = 0$), and the X_2 ($k_x = 0$, $k_y = 0.5$) points of the big BZ are folded back to the M point of the small BZ. An example is provided by the p_z bands in Fig. 10 which are antisymmetric to the plane of the square lattice (labelled "A"). The two at the Γ point in Fig. 10 correspond to one at Γ and another at M in Fig. 2. The degenerate pair at M comes from the X_1

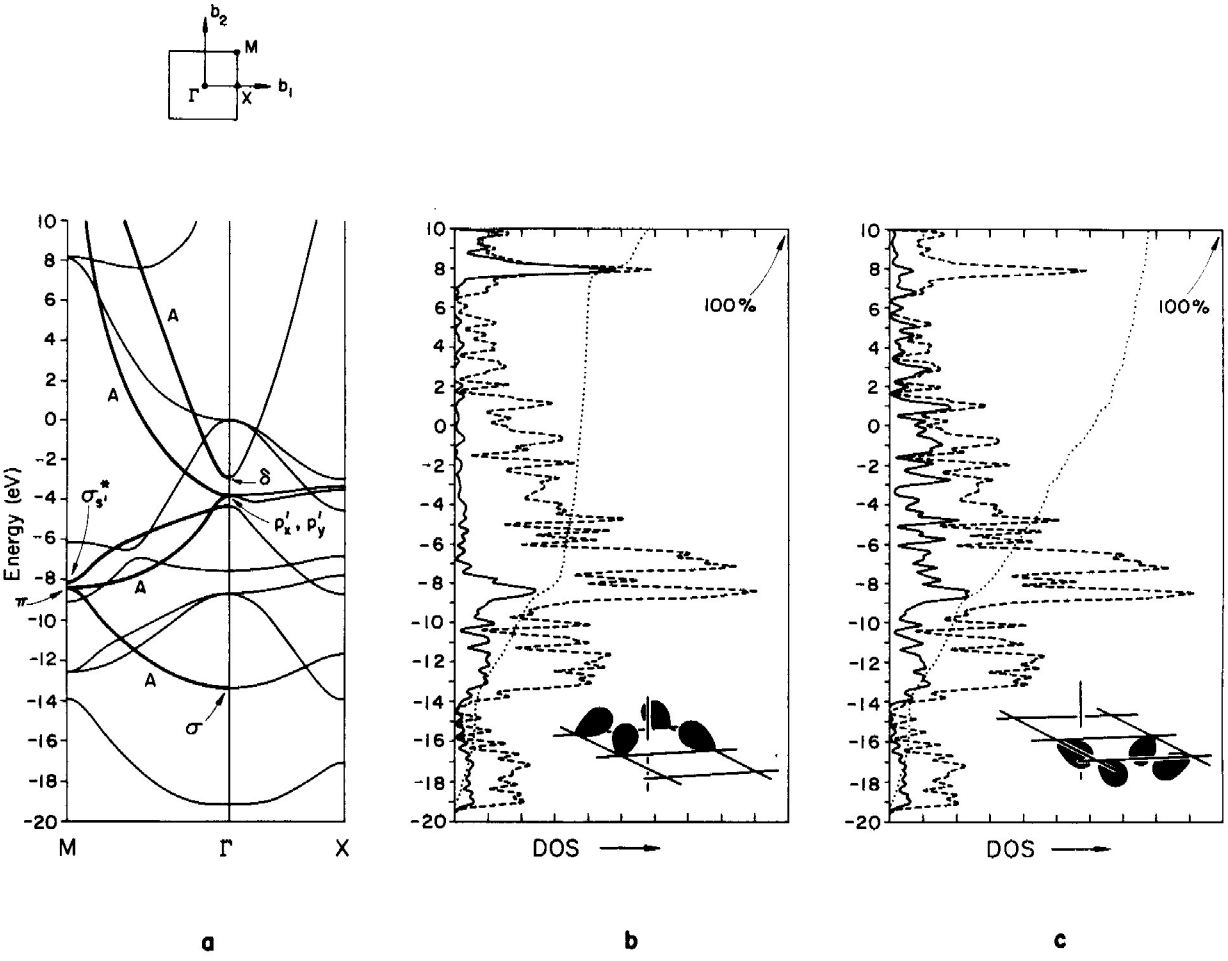

Fig. 9. (a) Band structures of a layer in $CeMg_2Si_2$ but made up from Al atoms. The heavy lines from M to Γ are the bands which are antisymmetric to the square lattice plane in the layer. The main contributions at M and Γ to those bands are indicated.
(b) Total density of states (dashed line) and the contribution from the basal hybrids pointing *to* the apical atom (solid line). The dotted line is the integration of those hybrid states.
(c) Total density of states (dashed line) and the contribution from the basal hybrids at the empty hollow pointing *away from* the apical atom (solid line).

and X_2 points of the small unit cell lattice. This is illustrated in **34**, where we identify the symmetry types (σ, π, δ) with respect to the apical position.

The bands in **34** can interact with the out-of-phase combination of the orbitals of the apical atoms sitting above and below the square hollow, shown in **35**. The basal orbitals corresponding to Γ, M interact with the apical ones, resulting in orbitals at the same k points, Γ, M. Note that by simply moving the apical Al′ atom in a $BaAl_4$ layer to an adjacent hollow, without changing the apical to basal atom distance, one attains a short apical to apical distance of

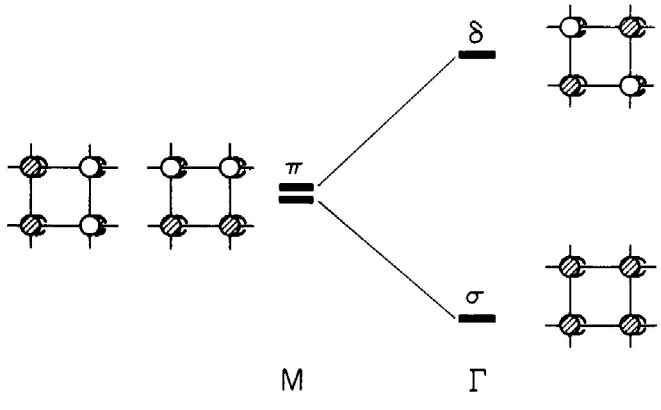

34

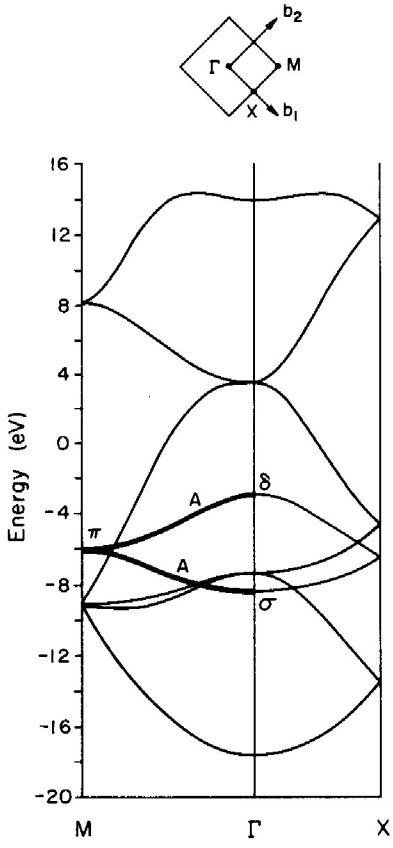

Fig. 10. Band structure of the two-dimensional square lattice in $BaAl_4$ as obtained by "folding back" Fig. 3. There are two atoms in the unit cell now.

2.90 Å, **36.** This is the geometry we used to calculate the band structure of Fig. 9. At this Al′–Al′ separation the out-of-phase apical p level combinations are between the basal π and δ type levels. This is where the orbitals were set in **35.** The other out-of-phase combination, $\sigma_{p_z'}^*$, **37** is high up in energy, well out of range for reasonable interaction.

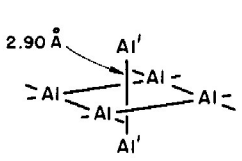

36

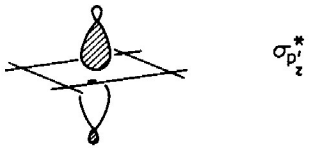

37

The resulting levels in **35** correspond to different points in the BZ. When we translate the results into a band structure scheme, what we obtain is **38** and **39.** **38** is the approximate band structure *before* the apical-basal interaction is turned on. The p_z bands of the basal atoms have the shape that we are familiar with, as in **34;** the apical bands are flat and essentially the out-of-phase combinations of the MO's of the apical Al′–Al′ pair. **39** is what we have *after* the interaction is turned on. The σ and π type orbitals from the basal atoms are pushed down and correspondingly $\sigma_{s'}^*$, and p_x', p_y' up in energy. The $\sigma_{s'}^*$ orbital, with the hybrid pointing away from the basal atoms, is not

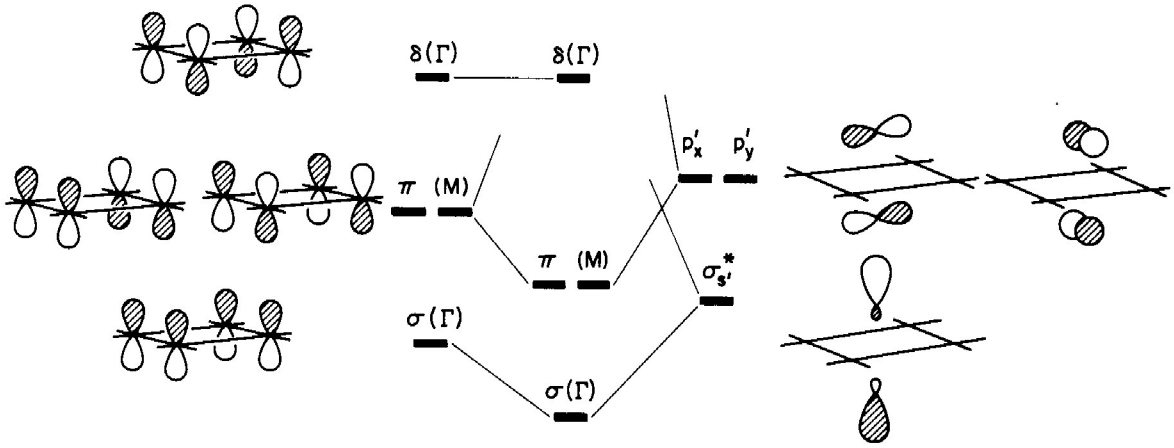

35

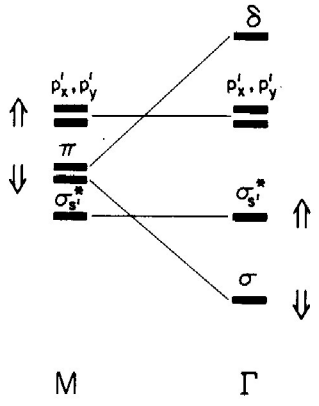

38

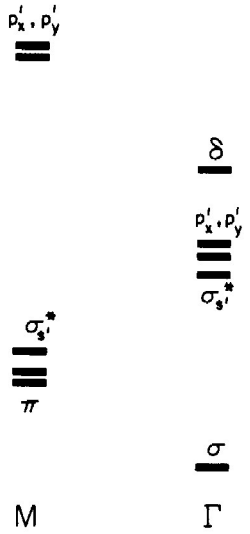

39

pushed as high as the p_x', p_y' orbitals. The δ type orbital from the basal atoms does not interact with the apical orbitals, neither do the $\sigma_{s'}^*$ at X nor the p_x', p_y' at Γ. They stay where they were. The arrows in **38** indicate the directions in which the orbitals will move *after* the interaction is turned on; **39** is the product of the level shift indicated in that way in **38.** When we connect the levels from the lowest one up, we will have the approximate band structure (the subset antisymmetric to the plane of the square lattice), **40.** This is that the antisymmetric bands look like from M to Γ in Fig. 9, except that the $\sigma_{s'}^*$ band connects and crosses the $\pi \rightarrow p_x, p_y$ band. This is due to another symmetry plane we have ignored so far, which is perpendicular to the plane of the square lattice and distinguishes $p_x' + p_y'$ and $\sigma_{s'}^*$ (symmetric) from $p_x' - p_y'$ (antisymmetric). We would rather not go into details, instead we point out that in this scheme of interaction there should be no band gap even within the antisymmetric bands, let alone for the symmetric bands in the complete band structure.

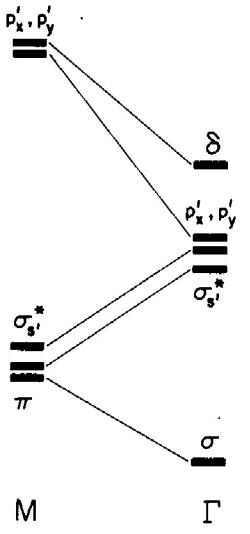

40

We now consider the perturbations that might be anticipated to the band structure in Fig. 9. The picture in **38, 39** can change if the apical atomic levels are well below the basal (square lattice) ones. This can happen when the apical atom is much more electronegative and the apical-apical distance shown in **36** is long so that the out-of-phase, antibonding apical combinations are close to the atomic ones in energy. Such a situation occurs in $CeMg_2Si_2$, where Si ($\chi = 1.9$) is much more electronegative than Mg ($\chi = 1.3$) [26] and the Si–Si distance *within* one layer is 3.19 Å (see **28**). In this case the interaction picture should have the form of **41.** All square lattice levels but the δ type one are destabilized by the low-lying apical atoms. A big gap should be present between

the apical and the basal levels, and a small gap between the apical p_x', p_y' and the $\sigma_{p_z'}^*$ bands.

Fig. 11 is the calculated band structure for the two-dimensional layer in $CeMg_2Si_2$. The antisymmetric bands (heavy lines) appear approximately they way we sketched them in **41,** with a small direct gap present between the apical p_x', p_y' and the $\sigma_{p_z'}^*$.

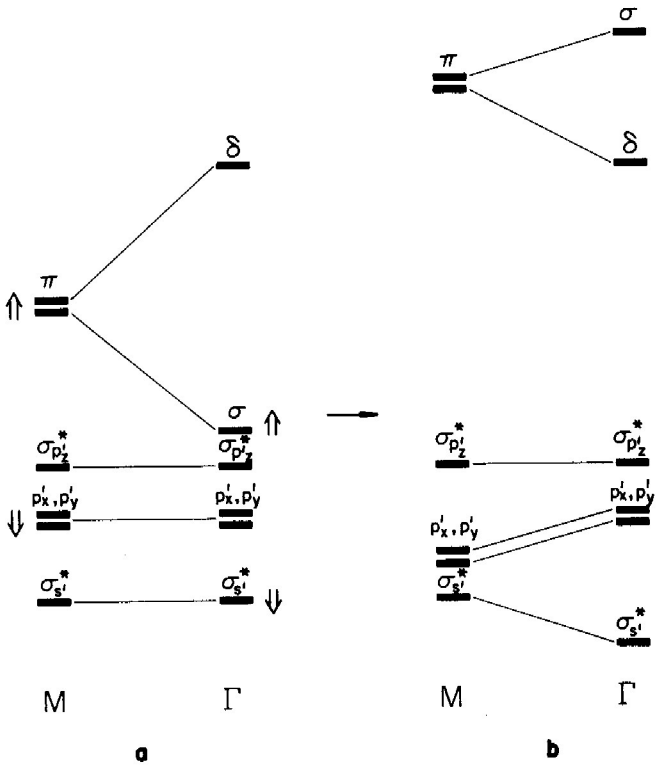

41

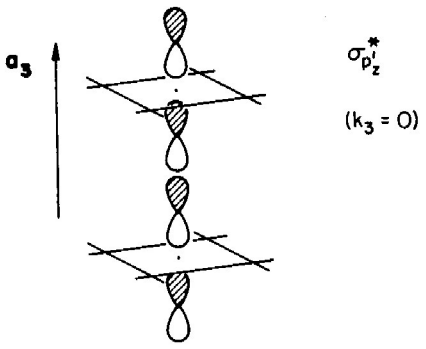

42

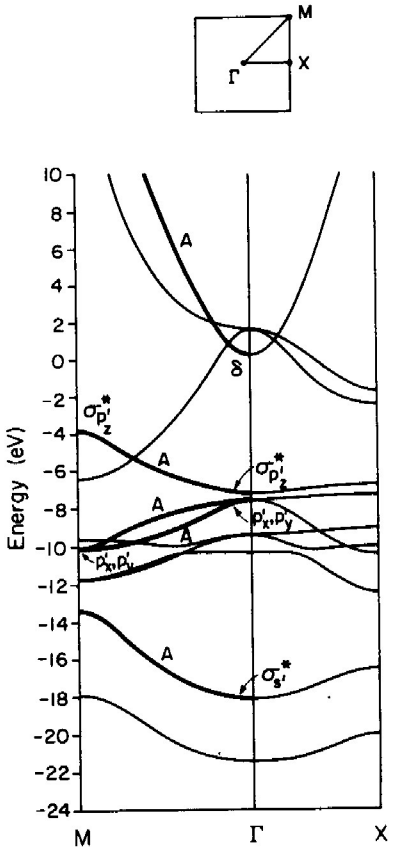

Fig. 11. Band structure of the two-dimensional Mg_2Si_2 layer in $CeMg_2Si_2$. The heavy lines from M to Γ are the bands which are antisymmetric to the square lattice plane in the layer. The main contributions to those bands are indicated at M and Γ.

When these layers are stacked into the three-dimensional $CeMg_2Si_2$ lattice, the $\sigma_{p_z'}^*$ band will be pushed out of the low-energy region by interaction with the same band in another layer, shown in **42.** There, the $\sigma_{p_z'}^*$ orbitals related by the translation a_3 have the same phase (for $k_3 = 0$), thus, the interlayer interaction is antibonding, as indicated by the arrow in **42.** In another region of the BZ, where $k_3 = 0.5$, the symmetric combination will be destabilized, **43,** and for intermediate k_3 the destabilized level is a mixture. The crystal knows itself which bands should be sent up in energy.

Fig. 12 is the calculated band structures for the three-dimensional Mg_2Si_2 lattice. Now there are only 3 antisymmetric bands below −6 eV. There is a very

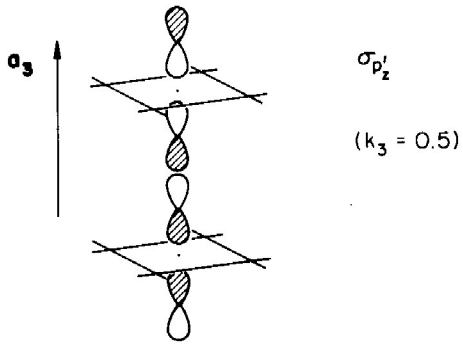

43

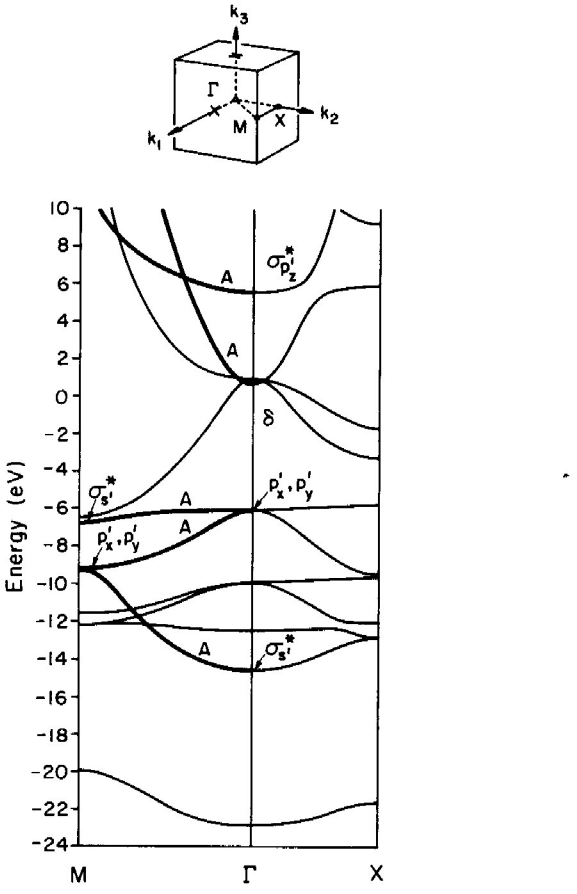

Fig. 12. Band structure of the three-dimensional Mg_2Si_2 lattice in $CeMg_2Si_2$. The heavy lines from M to Γ are the bands which are antisymmetric to the square lattice plane in $CeMg_2Si_2$.

small direct gap between the seventh and the eighth bands (around −6.6 eV at M), but there is no gap in the density of states.

We will summarize the results obtained so far. In the $BaAl_4$ structure the apical to basal atom interaction separates the 16 bands for the four Al atoms into two parts. The bonding and antibonding parts each consist of 8 bands in the two-dimensional layer, but the interlayer interaction destabilizes one of the low-lying bands. Thus for the final three-dimensional lattice there are seven low-lying bands of Al–Al bonding character and the good electron count is 14. For the $CeMg_2Si_2$ type structure there is no such clear separation of bands into regions, although increasing the electronegativity difference between the apical and basal atoms enhances such a possibility, so does the elongation of the intralayer apical-apical atomic bond. **44** is such a pictorial summary of what we have said.

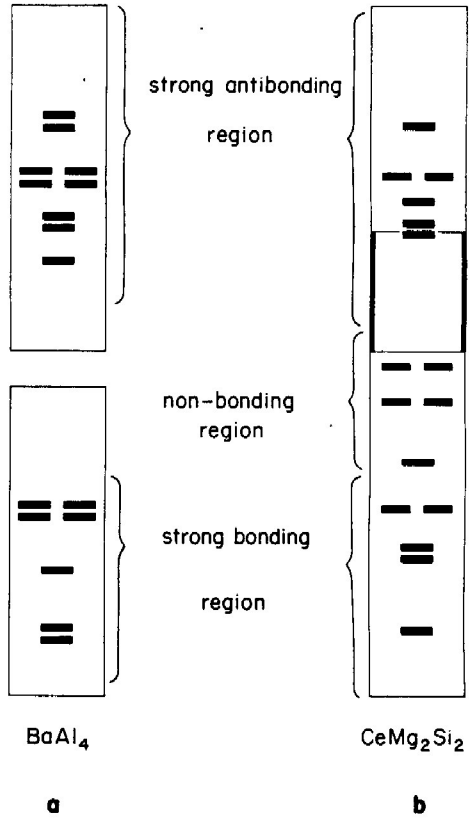

44

A consequence of the fact that the low-lying levels in $BaAl_4$ are more strongly apical to basal bonding and the high-lying bands more antibonding than the levels in a corresponding energy region in $CeMg_2Si_2$ is the following: For low electron filling the $BaAl_4$ structure is preferred. When the antibonding levels start to be filled, the preference will shift to the $CeMg_2Si_2$ structure, which has nonbonding levels in between the gap of **44a.** This is shown schematically in **45,** where we plot the difference in total energy for

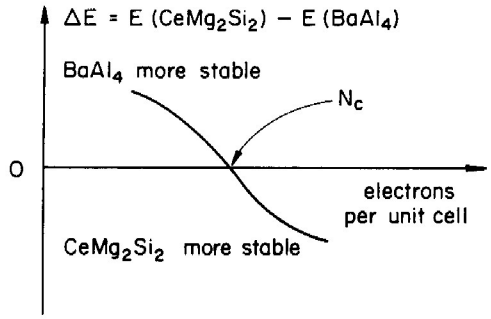

45

these two structures against electron filling. The critical electron count, N_c, should be slightly greater than 14. Our extended Hückel calculation gives $N_c = 18$ for Al atoms, but when the electronegativity difference and the intralayer apical-apical distance are increased, as in $CeMg_2Si_2$, N_c changes to 17. $CeMg_2Si_2$ itself has 15 or 16 electrons per unit cell, depending on the choice of oxidation state of Ce. There are quite a few $BaAl_4$ type compounds with 15 ($REAl_2Ga_2$) [10]

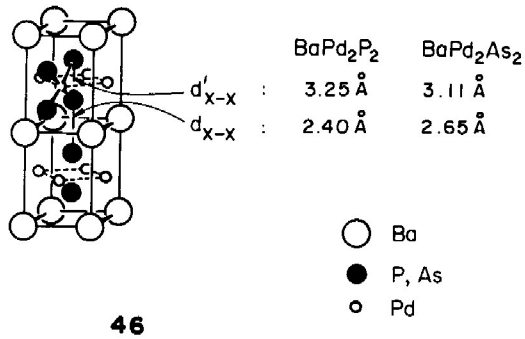

46

or even 16 electrons per unit cell ($SrAl_2Pb_2$) [30]. $CeMg_2Si_2$, on the other hand, is the only main group compound of its type to our knowledge. There are some transition metal compounds ($BaPd_2P_2$, $BaPd_2As_2$) of this type [31], in which the apical atoms (P or As) form bonds *within* the layer, **46.** The oxidation state for the metal is then $Ba^{2+}(Pd^{+})_2(P_2)^{4-}$. Had the pnicogens not formed the bond between them, the electron count would have been $Ba^{2+}(Pd^{2+})_2(P^{3-})_2$, a good d^8 configuration for the Pd^{2+} in the square planar coordination. The pnicogen-pnicogen bond in **46,** however, is slightly longer than a single bond distance (single bond distance: P–P = 2.21 Å, As–As = 2.43 Å), and there is a short Pd–Pd contact (3.01 Å). The packing requirement, on the other hand, may also play a role in determining the structure.

Formation of an apical-apical bond also occurs for $BaNi_2Si_2$, which is intermediate between $BaAl_4$ and $CeMg_2Si_2$ structures [32], **47.** The big cation Ba^{2+} interspersed in between the layers prevents the formation of the interlayer Si–Si bond, thus Si atoms,

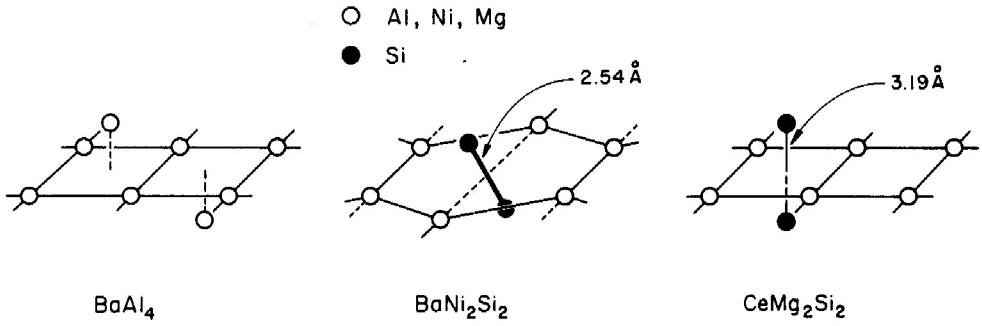

47

whose p orbital level is very close to the d band, form pairs within the layer. The proximity of the Si p orbital to the Ni d bands means that the antibonding σ^* orbital of the Si pair is above the Fermi level and empty, and the Si–Si bond is thus formed. One type of Ni–Ni bond is broken, giving way to the Si pair. The gain in stability upon Si–Si bond formation overrides the cost of breaking of the Ni–Ni bond, as confirmed by our calculations [34].

Al Metal

In the hypothetical "cleavage" process **2**, we had broken the FCC Al metal down to the two-dimensional layer **7** = **48** in order to understand the band structures, departing from the simplest two-dimen-

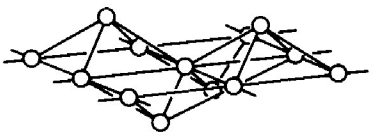

48

sional square lattice. This was accomplished. We also came to a simple alternative view of the band structure of the two-dimensional layer by thinking of the bonding pattern for the square pyramid at each hollow as a five-center, six-electron scheme. One a_1 and two e combinations of the basal hybrids interact with the hy_{in} hybrid and the p_x, p_y orbitals from the apical Al atom, resulting in three low-lying orbitals. The LUMO is the b_2 combination of the basal lone pairs, being of antibonding character and high up in energy. The other hybrid of the basal atom pointing away from the hollow, hy_{out}, **49**, is left free to interact, bond with the same type of orbital in another layer, which will result in another low-lying orbital for every two hollows.

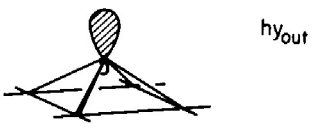

49

The reader may wonder what happens to the bands when assembling these two-dimensional layers together to form not $BaAl_4$, but the three-dimensional FCC Al lattice. This is exactly what we are going to do. But before we proceed, let us focus on some important geometric differences between the layer in $BaAl_4$ and that of Al metal.

The bond lengths in both layers are shown in **50.** In FCC Al metal, the equivalents of Al_a–Al_b and

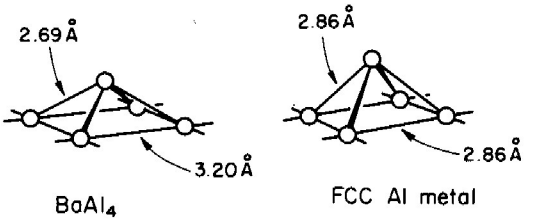

50

Al_b–Al_b are equal (see **51**). To put it another way, Al reconstructs, adjusts some of its bond distances and angles, when broken down to the two-dimensional layer by inserting Ba atoms. But why is the basal-basal bond elongated and the basal-apical shortened, and for instance, not the other way around?

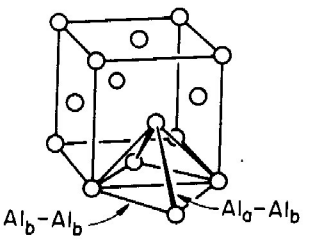

51

This can be easily understood based on our five-center, six-electron bonding pattern, **52.** On the left side there are four hybrids per hollow, symmetry adapted, ready to interact with the four orbitals from the apical atom. This total of eight orbitals corresponds to two Al atoms, and is occupied by 7 electrons in $BaAl_4$. The three lowest orbitals of the square pyramid are all apical-basal bonding. But what about their basal-basal bonding character?

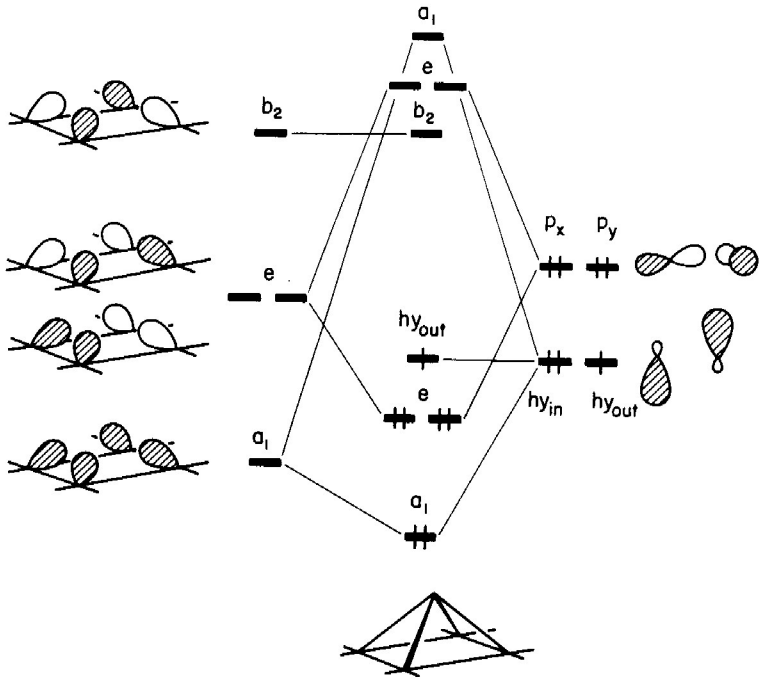

52

Only a_1 is Al_b-Al_b bonding, while e and hy_{out} are basal-basal nonbonding.

We expect the basal-basal bond to be weak. If we calculate the Al–Al overlap populations in an "unbiased" two-dimensional layer, with equal Al_b-Al_b and Al_a-Al_b distances, we obtain the result of **53.** The expectations on the bonding differential are confirmed.

53

The orbital diagram for the two-dimensional layer cleaved from Al metal should be topologically the same as **52,** except that without the Ba donating electrons, the hy_{out} level should be unfilled. Fig. 13 shows the calculated bands for that layer. The band structure for the two-dimensional Al layer in Fig. 13 resembles that of the $BaAl_4$ layer in Fig. 7. The only significant differences is the degree of dispersion of the bands above the gap. This is partly due to our different parameters for the isolated Al atom and the Al bulk metal (see the Appendix). But the empty upper

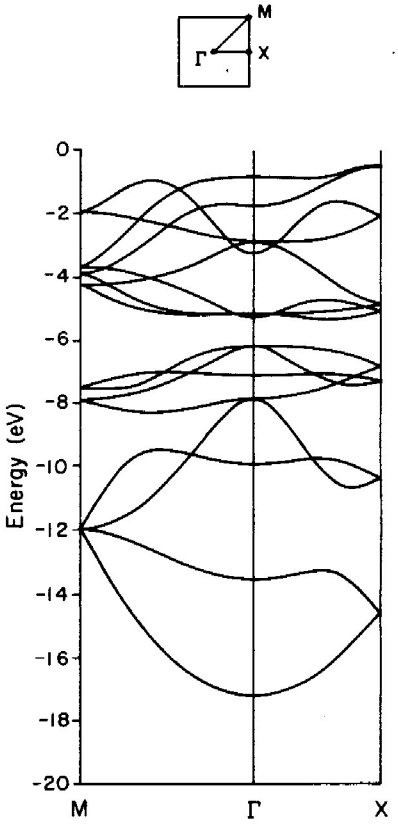

Fig. 13. Band structure of the two-dimensional layer from the FCC Al metal.

bands have no relevance to our present discussion. What is important is the fact that below the gap there are eight bands per two hollows, all of Al–Al bonding or non-bonding character.

We now stack the layers **48** together to form the FCC lattice. The hy_{out} orbital **49**, which points *away* from the hollow of the square lattice in the two-dimensional sheet, will now point *toward* the hollow of another layer. The orbital of the appropriate symmetry to interact in that layer is the a_1 of lower energy. Thus, we expect the hy_{out} orbital will be pushed up and there will be three bands per hollow which are of Al–Al bonding character. In other words, the bonding is maximized when there are six electrons per hollow, or three electrons per Al atoms since each hollow contains one apical and one basal atom.

Fig. 14 is the band structure for the three-dimensional Al FCC lattice stacked from two-dimensional layers. We do not see a "six bands below the gap" pattern. This is because every Al now has the same environment, being both "apical" and "basal", depending on where the k vector is in the Brillouin zone. We could say that the five-center, six-electron bonding pattern for a square pyramid could be thought of as "resonating" around the six possible square pyramids surrounding the apical atom in FCC Al metal.

In the delocalized band picture, the choice of the unit cell that we are led to by our layer construction (4 Al atoms) is not a good starting point. The simplest unit cell contains only one Al atom, and the band structures will be those in Fig. 14 but "unfolded", the reverse process to that in Fig. 7. However, the bonding character of the orbitals is the same, the physics does not change, no matter how we approach the construction of the electronic structure of the solid.

Fig. 15 is the COOP curve for Al metal. The Fermi level is almost exactly at the turning point at the COOP, the energy below which the states are Al–Al bonding and above which they are Al–Al strongly antibonding. In other words, three electrons per atom is the optimal count for main group FCC metals. Not surprisingly, Al has the highest cohesive

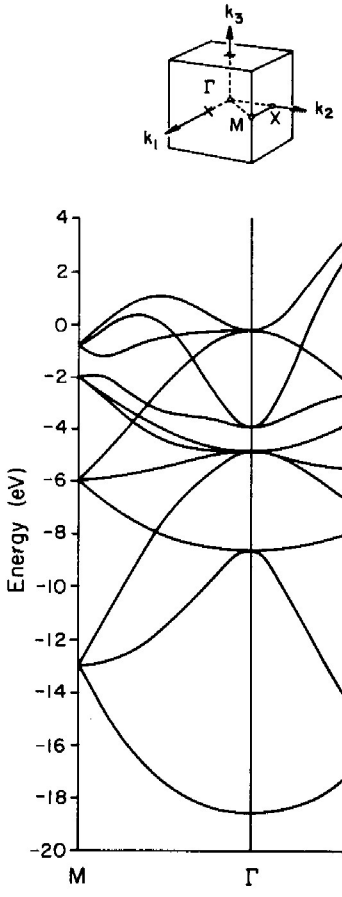

Fig. 14. Band structure of the three-dimensional FCC Al metal. The unit cell contains four atoms.

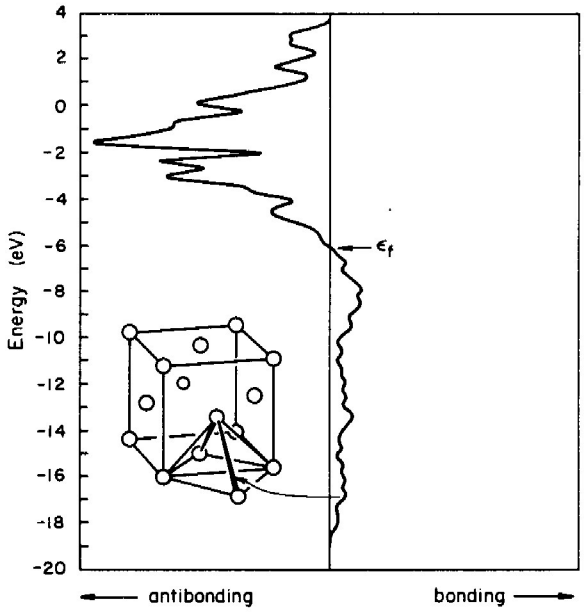

Fig. 15. Crystal Orbital Overlap Population curve for the shortest Al–Al bond in FCC Al metal.

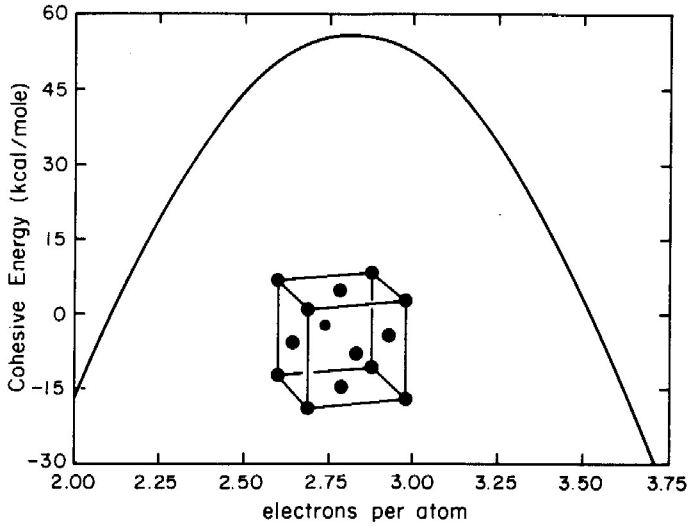

Fig. 16. Cohesive energy of a main group FCC metal as a function of the electron count. The curve is obtained by an extended Hückel rigid band model, using Al geometry and parameters.

energy (77 kcal/mol) among the main group FCC metals [35].

In fact, Al, together with Be (hcp), is the element which has the highest cohesive energy among *all* the main group elements on the metal side of the Zintl line in the Periodic Table. Our calculations reproduce the trend (Fig. 16), although the numerical value of the cohesive energy differs from the experimental one for Al. The values for other electron counts are calculated assuming a rigid band model, *i.e.*, using the Al geometry and parameters, and should not be taken too seriously when comparing to real experimental values for other metals. Only the trend has meaning in this rigid band approximation.

Appendix

The extended Hückel method [36] was used in all calculations. Table I lists the parameters. For the bulk Al metal, the exponents were contracted ($\zeta_s = 1.55$, $\zeta_p = 1.60$) to fit the experimental band structures [37], in particular the dispersion along $\Gamma \rightarrow X$ and the gap at the X point. A set of 28 or more k points was chosen according to ref. [38] to calculate DOS and COOP.

Table I. Extended Hückel parameters.

Orbitals	H_{ii} (eV)	ζ
Al 3 s	−12.3	1.17
3 p	− 6.5	1.17
Si 3 s	−17.3	1.38
3 p	− 9.2	1.38
Mg 3 s	− 9.0	1.1
3 p	− 4.5	1.1

We would like to thank Prof. Wolfgang Jeitschko for most helpful discussions. We are grateful to the National Science Foundation for its support of this work through grant CHE 8217227 and grant DMR 8217227 to the Materials Science Center at Cornell University. We thank Connie Baxter for the typing and Jane Jorgensen and Elisabeth Fields for the drawings.

[1] K. R. Andress and E. Alberti, Z. Metallkde. **27,** 126 (1935).
[2] a) W. B. Pearson, J. Solid State Chem. **56,** 278 (1985); b) F. Hulliger, Helv. Phys. Acta **58,** 216 (1985); c) R. Marchand and W. Jeitschko, J. Solid State Chem. **24,** 351 (1978); W. Jeitschko and B. Jaberg, ibid. **35,** 312 (1980); W. K. Hofmann and W. Jeitschko, ibid. **51,** 152 (1984).
[3] a) E. Parthé, B. Chabot, H. F. Braun, and N. Engel, Acta Crystallogr. **B 39,** 588 (1983); b) B. Chabot and E. Parthé, J. Less-Common Metals **97,** 285 (1984).
[4] B. Eisenmann, N. May, W. Müller, and H. Schäfer, Z. Naturfosch. **27b,** 1155 (1972).
[5] K. Klepp, H. Boller, and H. Völlenkle, Monatsh. Chem. **111,** 727 (1980).

[6] W. Dörrscheidt and H. Schäfer, J. Less-Common Metals **58,** 209 (1978); ibid. **70,** 1 (1980).
[7] a) E. Brechtel, G. Cordier, and H. Schäfer, Z. Naturforsch. **34b,** 251 (1979); ibid. **35b,** 1 (1980); J. Less-Common Metals **79,** 131 (1981);
b) G. Cordier, B. Eisenmann, and H. Schäfer, Z. Anorg. Allg. Chem. **426,** 205 (1976);
c) G. Cordier and H. Schäfer, Z. Naturforsch. **32b,** 383 (1976);
d) N. May and H. Schäfer, Z. Naturforsch. **29b,** 20 (1976);
e) W. Dörrscheidt, G. Savelsberg, J. Stöhr, and H. Schäfer, J. Less-Common Metals **83,** 269 (1982).
[8] a) F. Steglich, J. Aarts, C. D. Bredl, W. Lieke, D. Meschede, W. Franz, and H. Schäfer, Phys. Rev. Lett. **43,** 1892 (1979);
b) W. Lieke, U. Rauchschwalbe, C. D. Bredl, F. Steglich, J. Aarts, and F. R. de Boer, J. Appl. Phys. **53,** 2111 (1982);
c) W. Assmus, M. Herrmann, U. Rauchschwalbe, S. Regel, W. Lieke, H. Spille, S. Horn, G. Weber, F. Steglich, and G. Cordier, Phys. Rev. Lett. **52,** 469 (1984) and references cited therein.
For reviews on the physics, see
d) G. R. Stewart, Rev. Mod. Phys. **56,** 755 (1984);
e) C. M. Varma, Comments Solid State Phys. **11,** 221 (1985).
[9] H. F. Braun, J. Less-Common Metals **100,** 105 (1984).
[10] a) O. S. Zarechnyuk, P. I. Kripyakevich, and E. I. Gladyshevskii, Sov. Phys.-Crystallogr. **9,** 706 (1965);
b) E. V. Sampathkumaran, L. C. Gupta, R. Vijayaraghavan, T. K. Hatwar, M. N. Ghatikar, and B. D. Padalia, Mat. Res. Bull. **15,** 939 (1980);
c) M. N. Ghatikar, T. K. Hatwar, B. D. Padalla, E. V. Sampathkumaran, L. C. Gupta, and R. Vijayaraghavan, Phys. Stat. Sol. **106,** K 89 (1981);
d) T. K. Hatwar, B. D. Padalla, M. N. Ghatikar, and D. R. Chopra, ibid. **126,** 279 (1984).
[11] G. Cordier, E. Czech, and H. Schäfer, Z. Naturforsch. **39b,** 1629 (1984).
[12] O. F. Zmii and E. I. Gladyshevskii, Sov. Phys.-Crystallogr. **15,** 817 (1971).
[13] A. F. Wells, Structural Inorganic Chemistry, 5th Ed., Clarendon Press: Oxford 1984, pp. 269–270.
[14] J. Donohue, The Structures of the Elements, Robert E. Krieger Publishing Company: Malabar, Florida 1982, p. 82.
[15] The group notation is being changed in accord with recent actions by IUPAC and ACS nomenclature committees. A and B notation is being eliminated because of wide confusion. Group I becomes groups 1 and 11, group II becomes groups 2 and 12, group III becomes groups 3 and 13 *etc.*
[16] E. S. Makarov and L. S. Gudkov, Sov. Phys.-Crystallogr. **1,** 511 (1956).
[17] G. Bruzzone, Acta Crystallogr. **B 25,** 1206 (1969).
[18] a) R. Schäfer and W. Klemm, Z. Anorg. Allg. Chem. **312,** 214 (1961);
b) R. Thümmel and W. Klemm, ibid. **376,** 44 (1970).
[19] See W. Klemm, Proc. Chem. Soc. (London) **1958,** 329; H. Schäfer, B. Eisenmann, and W. Müller, Angew. Chem., Int. Ed. Engl. **12,** 694 (1973); H. Schäfer, Ann. Rev. Mat. Sci. **15,** 1 (1985).
[20] a) I. Imamura, J. Chem. Phys. **52,** 3168 (1970);
b) H. Fujita and I. Imamura, ibid. **53,** 4555 (1970);
c) S. Suhai, Biopolymers **13,** 1731 (1974);
d) Quantum Chemistry of Polymers – Solid State Aspects, J. Ladik and J.-M. André (eds), (D. Reidel Publishing Company, Dordrecht, Holland 1984) pp. 337–359.
For applications in solid state system, see
e) T. Hughbanks and R. Hoffmann, J. Am. Chem. Soc. **105,** 3528 (1983).
[21] C. Zheng and R. Hoffmann, to be published.
[22] Some other applications of the COOP curves may be found in: a) S. D. Wijeyesekera and R. Hoffmann, Organometallics **3,** 949 (1984);
b) M. Kertesz and R. Hoffmann, J. Am. Chem. Soc. **106,** 3453 (1984);
c) J.-Y. Saillard and R. Hoffmann, ibid. **106,** 2006 (1984).
[23] T. A. Albright, J. K. Burdett, and M.-H. Whangbo, Orbital Interactions in Chemistry, John Wiley & Sons, New York 1985, p. 241.
[24] In the three-dimensional $BaAl_4$ lattice the glide plane group is not Abelian, thus not represented by $\{e^{i\mathbf{k}\cdot\mathbf{R}}\}$.
[25] J. K. Burdett, J. Phys. Chem. **87,** 4368 (1983).
[26] See for example, J. E. Huheey, Inorganic Chemistry, 2nd Ed., Harper & Row: New York 1978, pp. 162–163.
[27] W. N. Lipscomb, Boron Hydrides, W. A. Benjamin: New York 1963, pp. 80–86.
[28] See also a) V. I. Minkin and R. M. Minyaev, Uspekhi Khimii **51,** 586 (1982); Russ. Chem. Rev. **51,** 332 (1982);
b) R. M. Minyaev und V. I. Minkin, Zh. Org. Khim. **18,** 2009 (1982); J. Org. Chem. USSR **18,** 1765 (1982).
[29] R. N. Grimes, F. E. Wang, R. Lewin, and W. N. Lipscomb, Proc. Natl. Acad. Sci. U.S. **47,** 996 (1961).
[30] N. May and H. Schäfer, Z. Naturforsch. **27b,** 864 (1972).
[31] A. Mewis, ibid. **39b,** 713 (1984).
[32] W. Dörrscheidt and H. Schäfer, ibid. **35b,** 297 (1979).
[33] For our analysis of bond formation and breaking in the solid state, see R. Hoffmann and C. Zheng, J. Phys. Chem., in press.
[34] C. Zheng and R. Hoffmann, unpublished results.
[35] The Structure and Properties of Matter, edited by T. Matsubara (ed.), Springer-Verlag: Berlin 1982, p. 124.
[36] R. Hoffmann, J. Chem. Phys. **39,** 1397 (1963); R. Hoffmann and W. N. Lipscomb, ibid. **36,** 2179, 3489 (1962); ibid. **37,** 2872 (1962); J. H. Ammeter, H.-B. Bürgi, J. C. Thibeault, and R. Hoffmann, J. Am. Chem. Soc. **100,** 3686 (1978).
[37] H. J. Levinson, F. Greuter, and E. W. Plummer, Phys. Rev. **B 27,** 727 (1983).
[38] J. D. Pack and H. J. Monkhorst, Phys. Rev. **B 16,** 1748 (1977).